AD-A116 277 ARMY MILITARY PERSONNEL CENTER ALEXANDRIA VA F/G 20/6
INTERSYMBOL INTERFERENCE IN A GRADED-INDEX FIBER OPTIC COMMUNIC--ETC(U)
APR 82 R L WACHTEL

UNCLASSIFIED NL

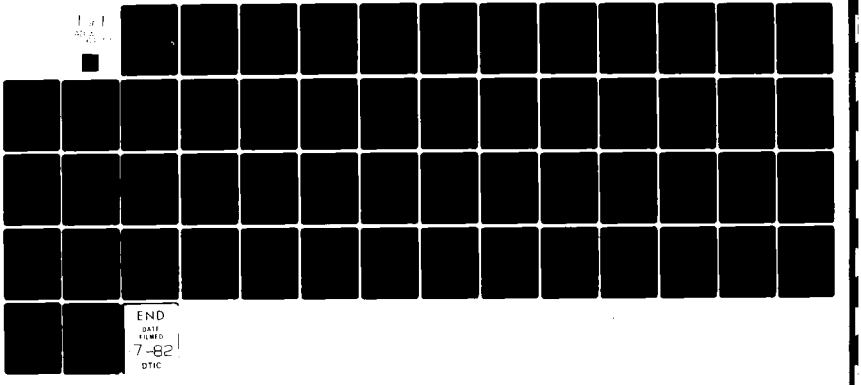

END
DATE FILMED
7-82
DTIC

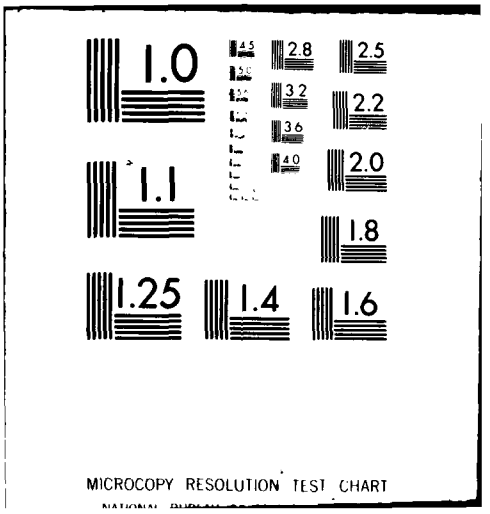
1.0
1.1
1.25
1.4
1.6
1.8
2.0
2.2
2.5
2.8
3.2
3.6
4.0
MICROCOPY RESOLUTION TEST CHART

(2)

INTERSYMBOL INTERFERENCE IN A GRADED-INDEX FIBER OPTIC COMMUNICATION SYSTEM

Raymond L. Wachtel, CPT
HQDA, MILPERCEN (DAPC-OPP-E)
200 Stovall Street
Alexandria, VA 22332

Final Report, April 1982

Approved for public release; distribution unlimited.

A thesis submitted to the University of Illinois at Urbana-Champaign in partial fulfillment of the requirements for the degree of Master of Science in Electrical Engineering.

SECURITY CLASSIFICATION OF THIS PAGE *(When Data Entered)*

REPORT DOCUMENTATION PAGE		READ INSTRUCTIONS BEFORE COMPLETING FORM
1. REPORT NUMBER	2. GOVT ACCESSION NO. AD-A116 297	3. RECIPIENT'S CATALOG NUMBER
4. TITLE *(and Subtitle)* INTERSYMBOL INTERFERENCE IN A GRADED-INDEX FIBER OPTIC COMMUNICATION SYSTEM		5. TYPE OF REPORT & PERIOD COVERED Final Report, April 1982
		6. PERFORMING ORG. REPORT NUMBER
7. AUTHOR(s) Raymond L. Wachtel		8. CONTRACT OR GRANT NUMBER(s)
9. PERFORMING ORGANIZATION NAME AND ADDRESS Student, HQDA, MILPERCEN (DAPC-OPP-E), 200 Stovall Street, Alexandria, VA 22332		10. PROGRAM ELEMENT, PROJECT, TASK AREA & WORK UNIT NUMBERS
11. CONTROLLING OFFICE NAME AND ADDRESS HQDA, MILPERCEN, ATTN: DAPC-OPP-E, 200 Stovall Street, Alexandria, VA 22332		12. REPORT DATE April 1982
		13. NUMBER OF PAGES 51
14. MONITORING AGENCY NAME & ADDRESS *(if different from Controlling Office)*		15. SECURITY CLASS. *(of this report)* UNCLASSIFIED
		15a. DECLASSIFICATION/DOWNGRADING SCHEDULE

16. DISTRIBUTION STATEMENT *(of this Report)*

Approved for public release; distribution unlimited.

17. DISTRIBUTION STATEMENT *(of the abstract entered in Block 20, if different from Report)*

18. SUPPLEMENTARY NOTES

Thesis, University of Illinois

19. KEY WORDS *(Continue on reverse side if necessary and identify by block number)*

WKB Solution for Graded-Index Fibers;
Optimum Gradient Index; Optimum Decision Threshold;
RMS Output Pulse Width; Receiver Error Rate;
Receiver Mathematical Model;
Probability of Error;

20. ABSTRACT *(Continue on reverse side if necessary and identify by block number)*

In this report, the effects of pulse dispersion and noise in a graded-index fiber optic communication system which utilizes pulse amplitude modulation are examined. It is shown that pulse dispersion can result in intersymbol interference and degraded error performance of the system. Expressions for RMS output pulse width, intersymbol interference, optimum threshold receiver level, and reeor probabilities are developed in terms of system parameters.

DD FORM 1 JAN 73 1473 EDITION OF 1 NOV 65 IS OBSOLETE

SECURITY CLASSIFICATION OF THIS PAGE *(When Data Entered)*

INTERSYMBOL INTERFERENCE IN A GRADED-INDEX FIBER OPTIC COMMUNICATION SYSTEM

BY

RAYMOND LOUIS WACHTEL

B.S., University of Illinois, 1972

THESIS

Submitted in partial fulfillment of the requirements
for the degree of Master of Science in Electrical Engineering
in the Graduate College of the
University of Illinois at Urbana-Champaign, 1982

Urbana, Illinois

ACKNOWLEDGEMENTS

I would like to express my appreciation to Dr. Chester S. Gardner, my thesis advisor, for his guidance, advice, and direction which contributed greatly to the completion of this thesis. I would also like to thank Richard C. Davis for his assistance and shared knowledge.

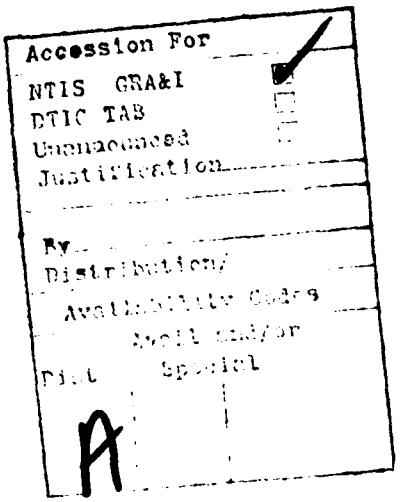

TABLE OF CONTENTS

CHAPTER 1

INTRODUCTION

Future communications systems will require information-carrying capacities of several hundred Mbits/sec over long link lengths. Graded-index fibers have assumed considerable importance since they offer the possibility of multimode propagation in a relatively large core fiber with low mode dispersion.

The performance of optical fibers for communications is chiefly determined by optical loss and by the temporal dispersion of light pulses caused by material and modal dispersion. Material dispersion occurs because the index of refraction varies as a function of wavelength. Modal dispersion results from the differences in the path lengths of the various transmission modes. Thus, material and modal dispersion determine the bandwidth and the information carrying capacity of the cable. For single mode step-index fibers, the diameter of the fiber is small, which causes difficulty in splicing and coupling to light sources. For a multimode step-index fiber with a large diameter core, modal dispersion severely limits the bandwidth and the fiber's utilization over long distances [1].

By varying the index of refraction across the radius of the fiber core, it is possible to compensate for the path length differences of the many modes carrying power in the fiber. Graded-index fibers thus combine the advantages of large core diameters with low modal dispersion.

In this report, we will examine the effects of pulse dispersion and noise in a graded-index fiber optic communication system which utilizes pulse amplitude modulation. It will be shown that pulse dispersion can result in intersymbol interference and degraded error performance of the system. Expressions for rms output pulse width, intersymbol interference, optimum receiver threshold levels, and error probabilities will be developed in terms of system parameters.

CHAPTER 2

PULSE DISPERSION IN GRADED-INDEX FIBERS

2.1 WKB Solution for Graded-Index Fibers

The propagation constants of a cylindrically symmetric waveguide with a arbitrary index profile can be obtained using the Wentzel-Kramers-Brillouin (WKB) approximation which is widely used in quantum mechanics [2]. Of primary interest will be the rms output pulse width which will be a function of both the material and modal disperson in the optical fiber. In the WKB analysis, the following assumptions are made:

1. The fiber core diameter is large so that numerous modes will be excited.
2. The index variation is small over distances of a wavelength.
3. All propagating modes carry equal amounts of energy.

The refractive index profile of the fiber can be modeled by

$$n(r) = n_o \left[1 - 2\Delta \left(\frac{r}{a}\right)^{\alpha} \right]^{1/2} \qquad r < a \qquad (2.1)$$

$$n(r) = n_o \left[1 - 2\Delta\right]^{1/2} \qquad r \geq a \qquad (2.2)$$

where

r = distance from the axis of the fiber

a = radius of the core

$\Delta = (n_o^2 - n_1^2)/2n_1^2$

n_o = refractive index at the fiber axis

n_1 = refractive index of the cladding

α defines the index gradient of the fiber.

It has been shown [3] for the above case that the total number of guided modes is given by

$$M = \left(\frac{\alpha}{\alpha+2}\right) a^2 n_o^2 k^2 \Delta \tag{2.3}$$

where k is the optical wavenumber. The group velocity for a given mode, m, is given by

$$V_g = \left[\frac{1}{c} \left(\frac{\partial \beta_m}{\partial k}\right)\right]^{-1} \tag{2.4}$$

where β_m is the propagation constant of the m'th mode in the direction parallel to the fiber axis. The time taken for energy propagating in the m'th mode to travel a distance L is therefore

$$\tau_m = \frac{L}{c}\left(\frac{\partial \beta_m}{\partial k}\right) \quad . \tag{2.5}$$

By using the WKB approximation it can be shown that [3]

$$\beta_m = n_o k \left[\, 1 - 2\Delta\left(\frac{m}{M}\right)^{\alpha/(\alpha+2)} \,\right]^{1/2} \quad . \tag{2.6}$$

Therefore, the propagation delay can be written

$$\tau_m = \frac{NL}{c}\left[1 - \left(\frac{\alpha-2-y}{\alpha+2}\Delta\left(\frac{m}{M}\right)^{\frac{\alpha}{(\alpha+2)}}\right) + \left(\frac{3\alpha-2-2y}{2(\alpha+2)}\Delta^2\left(\frac{m}{M}\right)^{\frac{2\alpha}{(\alpha+2)}}\right) + O(\Delta^3)\right] \tag{2.7}$$

where

$$y = \frac{-2n_o\lambda}{N\Delta}\left(\frac{\partial\Delta}{\partial\lambda}\right) \tag{2.8}$$

and the group index is defined as

$$N = n_o + \lambda\left(\frac{\partial n_o}{\partial\lambda}\right) \tag{2.9}$$

λ = wavelength of light transmitted.

The mode number, m, used above is related to the double quantum-number $LP_{\ell'm'}$ system of labeling by the simple approximation

$$m \simeq (2m' + \ell' + 1)^2 \quad . \tag{2.10}$$

For the purposes of specifying the fiber bandwidth for a digital system, the rms pulse width is of primary importance and is given by

$$\sigma = \left[\langle \tau_m^2 \rangle - \langle \tau_m \rangle^2\right]^{1/2} \tag{2.11}$$

$$= \left[\sigma_I^2 + \sigma_M^2\right]^{1/2} + O\left(\frac{\sigma_s^3}{\lambda_o^3}\right) \tag{2.12}$$

where σ_I is the term due to intermodal dispersion and is given by

$$\sigma_I = \frac{LN\Delta}{2c}\left(\frac{\alpha}{\alpha+1}\right)\left(\frac{\alpha+2}{3\alpha+2}\right)^{1/2}\left[c_1^2 + \frac{4c_1c_2\Delta(\alpha+1)}{2\alpha+1} + \frac{4c_2^2\Delta^2(2\alpha+2)^2}{(5\alpha+2)(3\alpha+2)}\right]^{1/2} \tag{2.13}$$

$$c_1 = \frac{\alpha - 2 - y}{\alpha + 2} \tag{2.14}$$

$$c_2 = \frac{3\alpha - 2 - 2y}{2(\alpha+2)} \quad . \tag{2.15}$$

The σ_M term is due to intramodal dispersion and equals

$$\sigma_M = \frac{\sigma_s}{\lambda_o}\left[-\lambda^2\left(\frac{d^2n_o}{d\lambda^2}\right)^2 - 2\lambda^2\left(\frac{d^2n_o}{d\lambda}\right)(N\Delta)\left(\frac{\alpha-2-y}{\alpha+2}\right)\left(\frac{2\alpha}{2\alpha+2}\right) + (N\Delta)^2\left(\frac{\alpha-2-y}{\alpha+2}\right)^2\left(\frac{2\alpha}{3\alpha+2}\right)\right]^{1/2} \tag{2.16}$$

where the rms spectral width of the source is defined by

$$\sigma_s = \left[\int_o^\infty d\lambda\ (\lambda - \lambda_o)^2\ S(\lambda)\right]^{1/2} \tag{2.17}$$

and the mean source wavelength is given by

$$\lambda_o = \int_o^\infty d\lambda\lambda S(\lambda) \quad . \tag{2.18}$$

The rms pulse width has been separated into an intermodal and an intramodal component. The intermodal term results from delay differences among the various modes propagating in the fiber. The intramodal component represents an average of the pulse broadening within each mode and arises from material and waveguide dispersion. With the

proper choice of α in a graded-index fiber, the intermodal dispersion is small and the intramodal effects caused by material dispersion predominate. The lower limit of the output rms pulse width is

$$\sigma_{min} \simeq \frac{\sigma_s}{\lambda_o}\left(\lambda_o^2 \quad \frac{d^2 n_o}{d\lambda^2}\right) \quad . \tag{2.19}$$

2.2 Selection of the Optimum Gradient Index

The total rms pulse spreading can be calculated [2] using (2.12), (2.13), and (2.14). In Figure 1, this rms

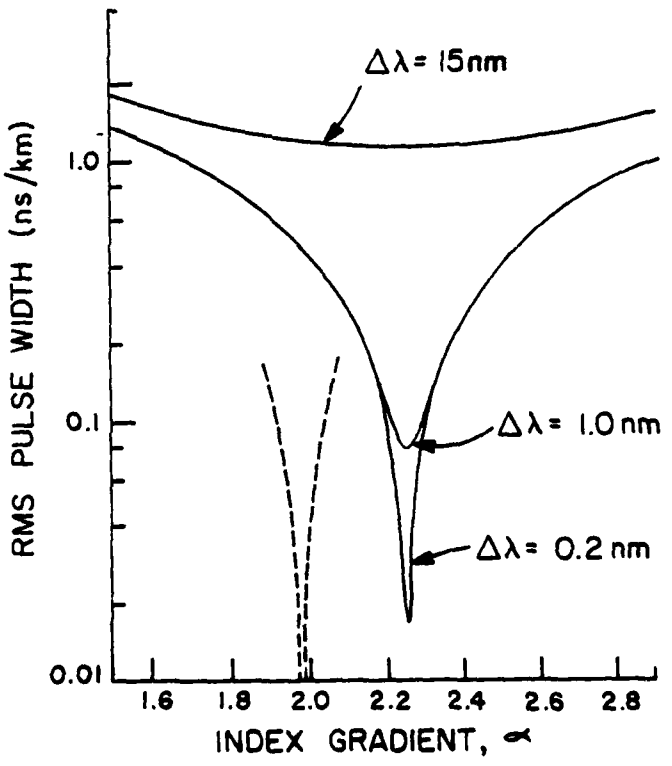

Figure 1. Calculated rms pulse spreading in a graded fiber as a function of the parameter α.

pulse width is shown as a function of α for three types of GaAs sources all operating at 900 nm but having different spectral bandwidths. The fiber parameters are characteristic of TiO_2 doped silica guide with $\Delta = 0.0059$. The three curves correspond to an LED, an injection laser, and a distributed feedback laser having typical rms spectral widths of 15 nm, 1.0 nm, and 0.2 nm respectively. For comparison, the dashed curve represents the predicted rms width if material dispersion and intramodal broadening are ignored. In this case, (2.13) alone is used to compute pulse spreading. The figure demonstrates that pulse dispersion, with an LED source, has a lower limit of approximately 1.0 ns/km and is set by the material dispersion of the fiber. Using a laser source, the pulse dispersion approaches 0.02 ns/km.

In order to minimize the pulse dispersion, an optimum index gradient must be selected which will decrease the intermodal dispersion to a minimum. In (2.13), if we set y=0, which corresponds to ignoring material dispersion, the minimum dispersion occurs for α of nearly 2. For $y \neq 0.0$, the minimum occurs at approximately 2.23 and is given by

$$\alpha_{min} = 2 + y - \Delta \left(\frac{(4+y)(3+y)}{5+2y} \right) . \qquad (2.20)$$

Since the optimal α varies strongly with the wavelength of the source, the output RMS pulse width is dependent upon the source wavelength for a particular cable.

2.3 Accuracy of the WKB Analysis

Although the WKB analysis is relatively simple and comprehensive, it is an approximation and results in errors for modes close to cutoff [4]. In reality, these modes always carry less power than the modes that are well guided. This fact means that predicted values of rms pulse width will not always correspond to experimental values. In the WKB analysis, the maximum delay difference between propagating modes was approximately $T\Delta^2/2$, where T and Δ denote the propagation time and the relative refractive index respectively. By more exact analysis, we find that the delay time differences between well-confined modes and modes close to cutoff approach $T\Delta$. Since we have assumed a small Δ, in this case 0.0059, inaccuracies of this magnitude can be ignored for cable lengths under discussion.

In addition, the WKB analysis predicts an optimal index gradient. In practice, it is difficult to produce an optimal index gradient in a fiber many kilometers long. For the LED source, pulse broadening of less than 1.5 nsec/km can be achieved if α is within 25% of the optimal value. For the injection laser, an α within 5% of the optimal value will give widths less than 0.2 nsec/km, and for the distributed feedback laser, widths of 0.05 nsec/km are predicted if 1% control on α can be achieved.

2.4 RMS Output Pulse Width as a Function of the Fiber Parameters

The temporal spreading experienced by a pulse of light as it propagates along a graded index optical fiber is characterized in terms of the dispersion parameters σ_I and σ_M given in (2.13) and (2.16). We can express the output pulse width, T_{out}, in terms of the individual fiber parameters as

$$(T_{out})_{rms} = \left[(z\sigma_I)^2 + (z\sigma_M)^2 + T_i^2 \right]^{1/2} \qquad (2.21)$$

where z is the fiber length and T_i is the rms input pulse width. With the optimal choice of α for the graded index fiber, the intermodal dispersion is small and the dispersion term, σ_M, predominates. Therefore the output pulse width can be expressed as

$$(T_{out})_{rms} = \left[(z\sigma_M)^2 + T_i^2 \right]^{1/2} . \qquad (2.22)$$

The expression for σ_M, (2.16), can be evaluated using data listed in [2].

In Figures 2 and 3, the rms output pulse width is plotted as a function of the fiber length, z, for various values of rms input pulse width. A GaAs LED source with a line width of 15 nm and wavelength of 900 nm is assumed. When T_i is significantly larger than 20 nsec, the T_i^2 term is dominant in (2.22) and T_{out} increases very slowly with increasing z.

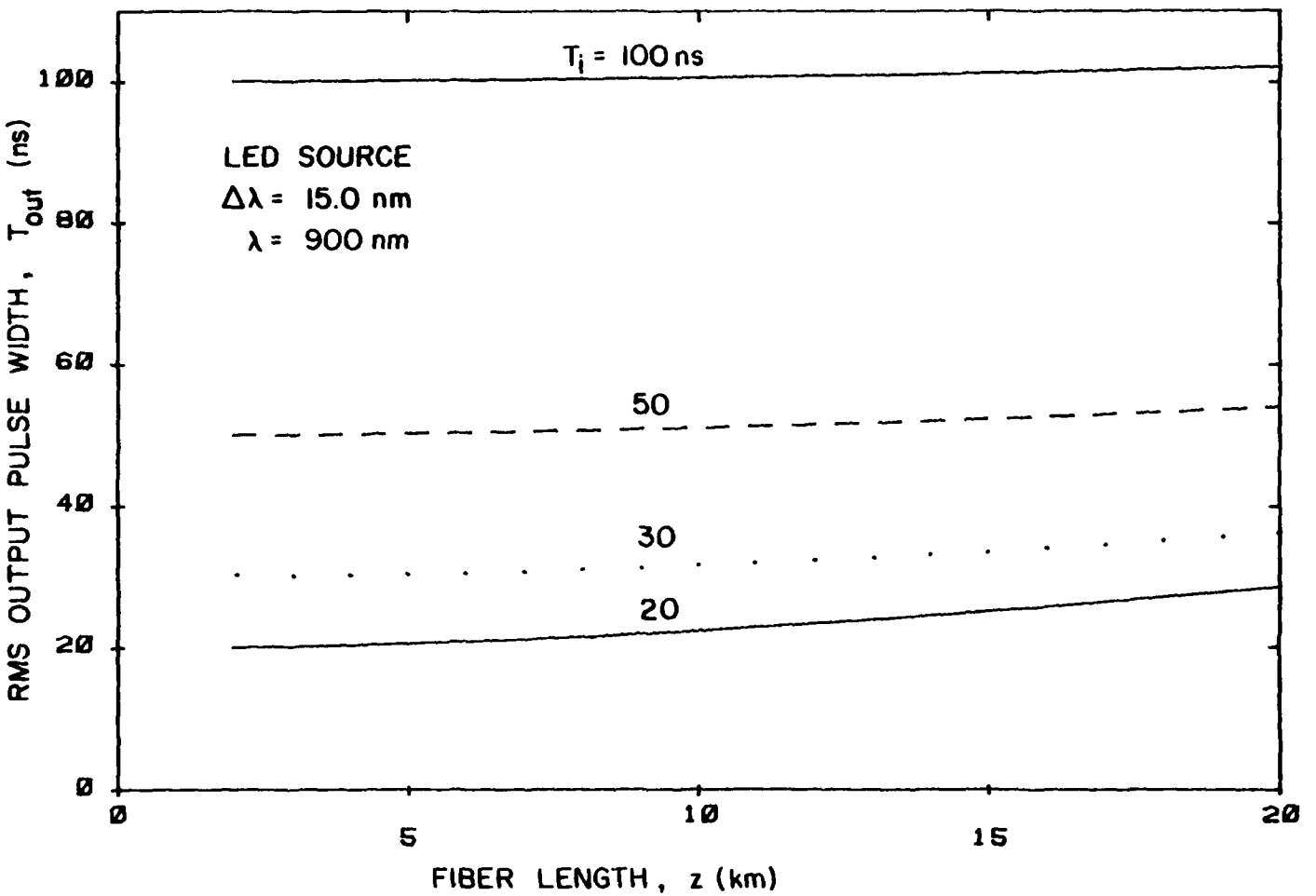

Figure 2. RMS output pulse width, T_{out} (nanoseconds) as a function of the fiber length, z (kilometers) for various values of rms input pulse width, T_i (nanoseconds).

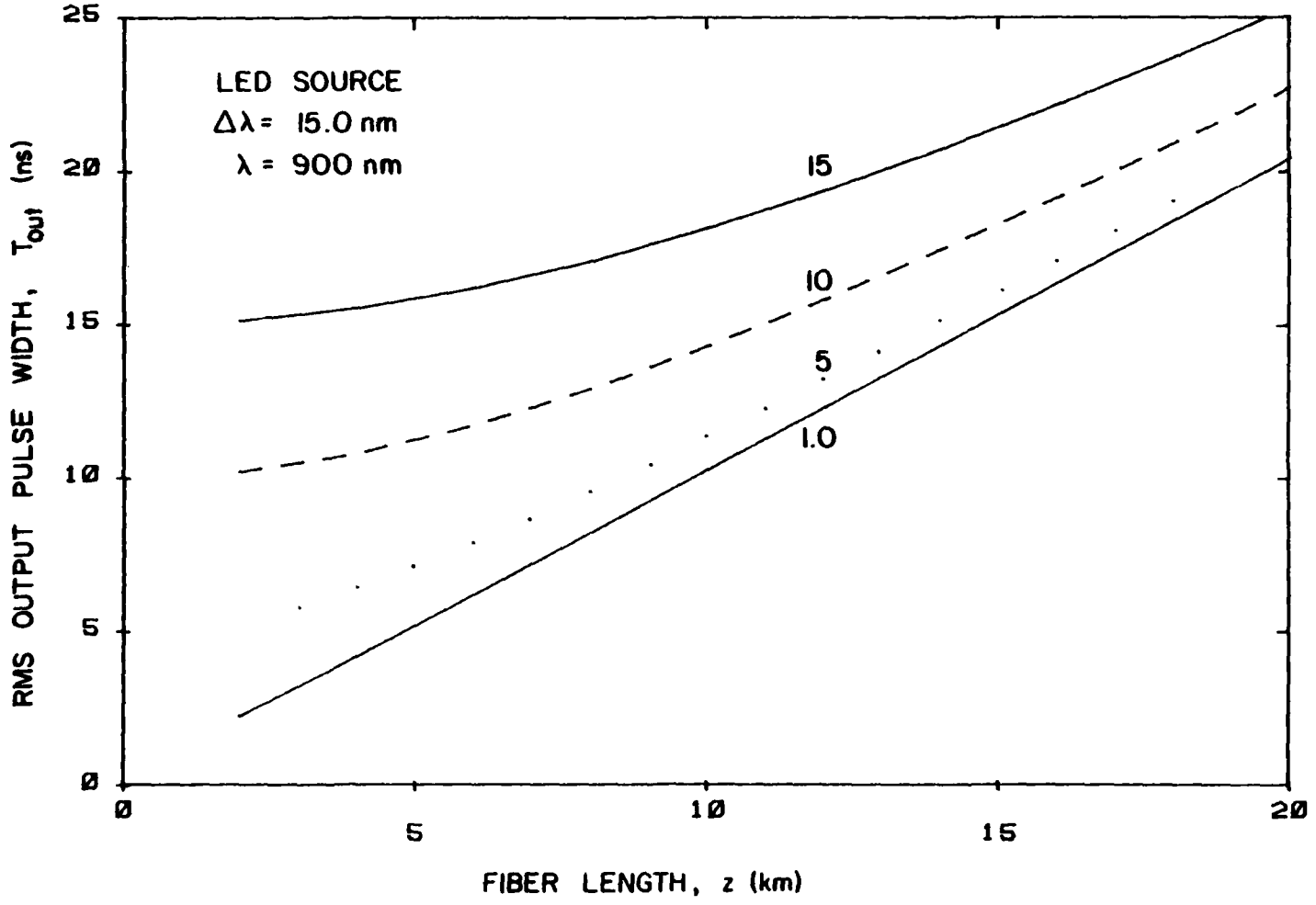

Figure 3. RMS output pulse width, T_{out} (nanoseconds) as a function of the fiber length, z (kilometers) for various values of rms input pulse width, T_i (nanoseconds).

In Figures 4 and 5, T_{out} is again plotted as a function of z and T_i. A GaAs laser source with a wavelength of 900 nm and a line width of 1.0 nm is assumed. The temporal spreading experienced as a function of increasing z is similar to the results obtained with the GaAs LED source. The magnitudes of T_{out} and T_i differ in these two cases because of the larger source line width of the LED source.

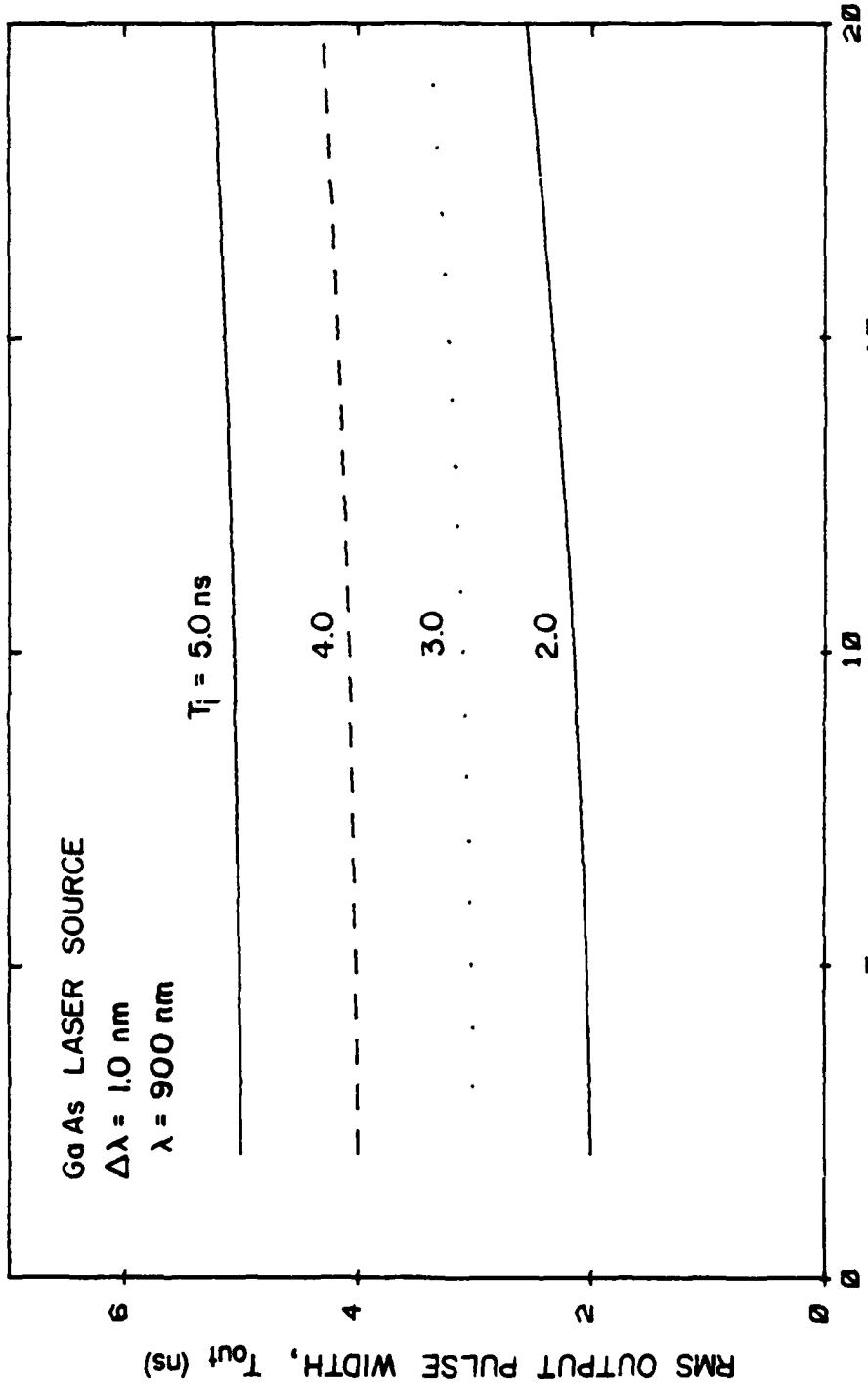

Figure 4. RMS output pulse width, T_{out} (nanoseconds) as a function of the fiber length, z (kilometers) for various values of rms input pulse width, T_i (nanoseconds).

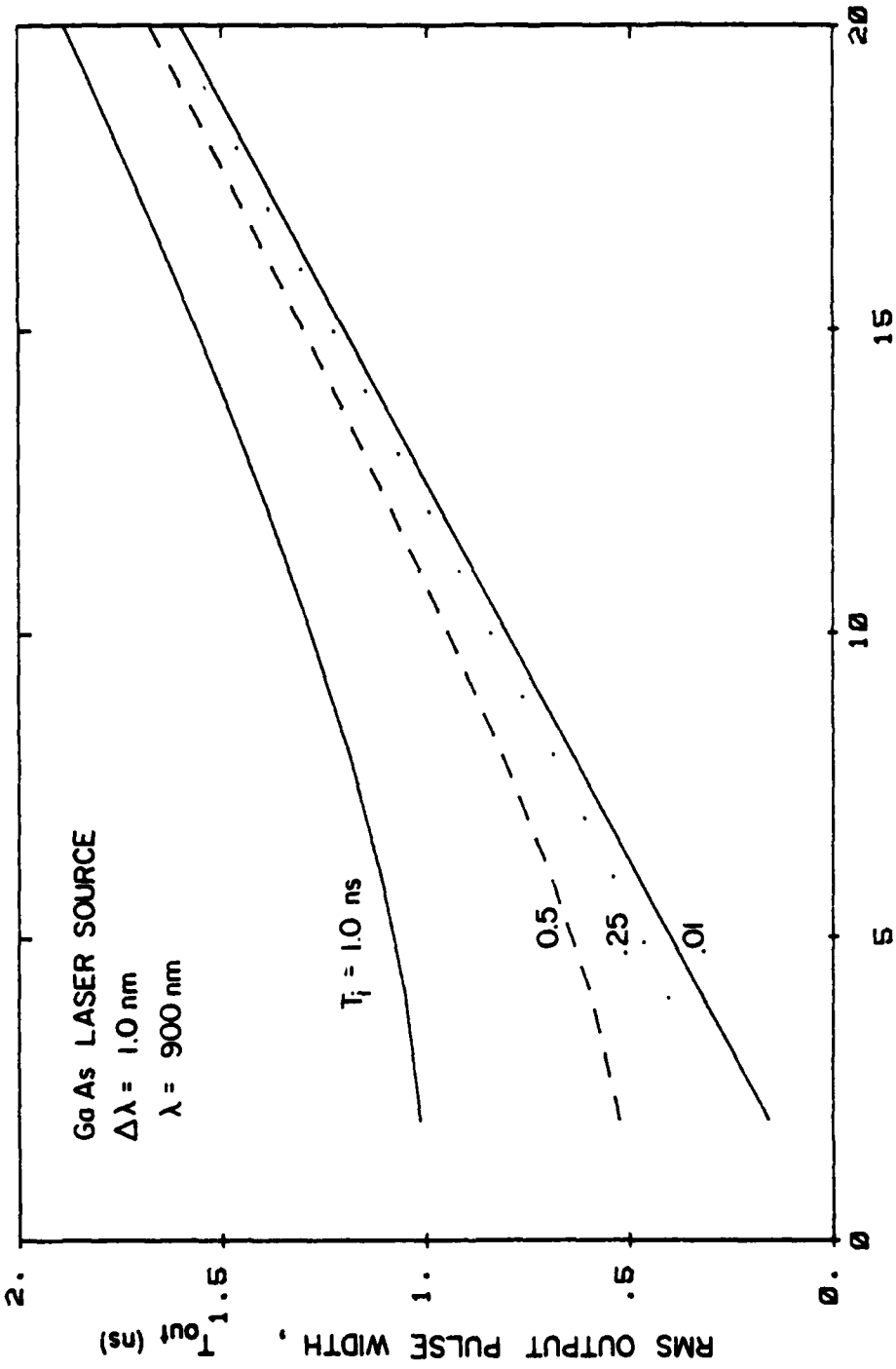

Figure 5. RMS output pulse width, T_{out} (nanoseconds) as a function of the fiber length, z (kilometers) for various values of rms input pulse width, T_i (nanoseconds).

CHAPTER 3

ANALYSIS OF AN OPTICAL DIGITAL RECEIVER

3.1 Mathematical Model of the Receiver

In fiber optical systems, the detector output produced by the optical power impinging upon an avalanche photodiode is an inhomogeneous, non-stationary shot noise process [5]. It is assumed that the optical power, p(t), impinging upon the avalanche photodiode's p-n junction is a truncated stream of independent binary digits. A mathematical model of an optical digital receiver is depicted in Figure 6. It consists of a p-n junction followed by a random multiplier with a known electron output probability density function followed by a filter. Arrival or absence of a transmitted pulse is decided by a comparator. An incorrect decision may be caused by thermal noise, intersymbol interference, shot noise, or dark current.

The current x(t) is comprised of $x_s(t)$, the signal current from the random multiplier output, and the Gaussian noise current $x_{th}(t)$. x(t) is given by

$$x(t) = x_s(t) + x_{th}(t) \quad . \tag{3.1}$$

$x_s(t)$ is an inhomogenous, non-stationary shot noise process given by

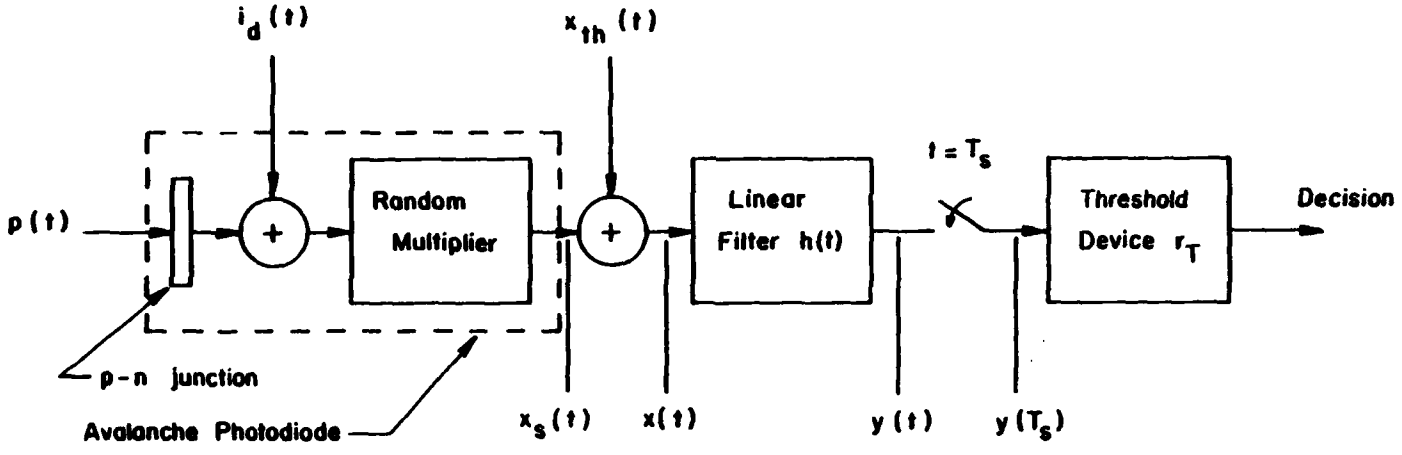

Figure 6. Mathematical model of an optical digital receiver.

$$x_s(t) = \sum_{v=1}^{V(t)} g_v \, \delta(t-t_v) \tag{3.2}$$

where t_v is the time release of the vth electron from the p-n junction. V(t) is a random number of these electrons which occur in a time interval up to t and g_v are statistically independent multiplicative random variables corresponding to the random multiplication and random gains encountered in the multiplier.

The p-n junction produces primary electrons in response to the impinging optical power, p(t), and due to thermal effects. The rate at which primary electrons are produced obeys Poisson Statistics with an average rate of

$$\lambda(t) = \lambda_s(t) + \lambda_d \tag{3.3}$$

where

$$\lambda_s(t) = \frac{\eta}{hf} p(t) \tag{3.4}$$

and

η = junction quantum efficiency

h = Planck's constant

f = optical frequency

λ_d = dark current "counts" per second.

$\lambda(t)$ is only the average rate at which electrons are produced. The probability that exactly k electrons are produced in any interval T seconds long is given by

$$P[k,(t_o,t_o+T_s)] = \frac{\mu^k e^{-\mu}}{k!} \tag{3.5}$$

where

$$\mu = \int_{t_o}^{t_o+T_s} \lambda(t)dt \quad . \tag{3.6}$$

Given p(t), the number of electrons produced in any interval is statistically independent of the number produced in any other adjacent interval [6]. p(t) is assumed to be of the form of a digital pulse stream given by

$$p(t) = \sum_{i=-\infty}^{\infty} d_i < |S_o(t-iT_s)|^2 > \tag{3.7}$$

where

d_i = sequence of independent equiprobable data symbols

T_s = signaling interval

$<|S_o(t-iT_s)|^2>$ = fiber distorted pulse shape which is positive for all t.

We shall assume

$$\int_{-\infty}^{\infty} <|S_o(t-iT_s)|^2> = 1 \ . \tag{3.8}$$

Thus, d_i is the energy in the ith pulse. We will assume that the fiber distorts the pulse enough so as to cause intersymbol interference (ISI). In the presence of ISI, $\lambda_s(t)$ can be broken into two parts:

$$\lambda(t) = \frac{\eta}{hf}\left[d_o \langle |S_o(t)|^2 \rangle + \sum_{\substack{i=-\infty \\ i\neq 0}}^{\infty} d_i \langle |S_o(t-iT_s)|^2 \rangle\right] + \lambda_d . \tag{3.9}$$

The zeroth term in the summation represents the photon arrival rate for the pulse under detection. The signaling slots containing the ISI components are comprised of the remaining terms.

3.2 Statistics of the Receiver Output

In Figure 6, the current x(t), is linearly filtered. h(t) is the impulse response of the filter, and y(t) is the filter output. The signal component of this output (due to the nonuniform shot noise) is given by

$$y_s(t) = x_s(t) * h(t) = \sum_{n=-\infty}^{\infty} g_n h(t-t_n) . \tag{3.10}$$

The mean and variance of the signal at the receiver output can be calculated using Campbell's theorem [7]:

$$E[y_s(t)] = \lambda(\tau) * h(\tau) = \int_{-\infty}^{\infty} d\tau \, \frac{\eta}{hf} \, p(\tau) \, h(t-\tau) \tag{3.11}$$

$$C_{y_s}(t_1,t_2) = \int_{-\infty}^{\infty} d\tau \, \frac{\eta}{hf} \, p(\tau) h(t_1-\tau) h(t_2-\tau) \tag{3.12}$$

where C_{y_s} is the covariance of the received signal. The impulse response of the filter is described by

$$h(\tau) = \begin{cases} \bar{h} & |\tau| \leq \frac{T_s}{2} \\ 0 & \text{elsewhere} \end{cases} \tag{3.13}$$

and

$$h(t - \tau) = \bar{h} \ \text{rect} \left(\frac{t - \tau}{T_s} \right) \tag{3.14}$$

where h is a constant. The region over which $h(t-\tau)$ is non-zero satisfies the inequality

$$|t - \tau| \leq \frac{T_s}{2} \tag{3.15}$$

which redefines the limits of integration to

$$t - \frac{T_s}{2} < \tau < t + \frac{T_s}{2} \ . \tag{3.16}$$

By using the above results, the mean and variance of $y_s(t)$ can be written as

$$E[y_s(t)] = \int_{t - \frac{T_s}{2}}^{t + \frac{T_s}{2}} d\tau \ \frac{\eta \bar{h}}{hf} \ p(\tau) \tag{3.17}$$

$$\text{Var}[y_s(t)] = \int_{t - \frac{T_s}{2}}^{t + \frac{T_s}{2}} d\tau \ \frac{\eta \bar{h}^2}{hf} \ p(\tau) = \bar{h} \ E[y_s(t)] \tag{3.18}$$

where $p(\tau)$ is given by (3.7). If the sequence of data symbols is known, the mean and variance of the signal component of the output become

$$E[y_s(t)|d_i] = \int_{t-T_s/2}^{t+T_s/2} d\tau \frac{\bar{h}}{hf} \sum_{i=\infty}^{\infty} d_i \langle |S_o(\tau - iT_s)|^2 \rangle \qquad (3.19)$$

$$Var[y_s(t)|d_i] = \bar{h}\, E[y_s(t)|d_i] \quad . \qquad (3.20)$$

The thermal noise component of the output is $y_{th}(t)$ where

$$y_{th}(t) = \int_{-\infty}^{\infty} d\tau \; x_{th}(\tau)\, h(t-\tau) \; . \qquad (3.21)$$

The thermal noise is uncorrelated with zero mean. The variance of the filtered thermal noise at the receiver output is

$$\sigma_{th}^2 = \int_{-\infty}^{\infty} dt \, \frac{N_o}{2} \, h^2(t) \qquad (3.22)$$

which reduces to

$$\sigma_{th}^2 = \int_{o}^{T_s} dt \, \frac{N_o}{2} \, \bar{h}^2 = \frac{N_o T_s \bar{h}^2}{2} \qquad (3.23)$$

where $N_o/2$ is the two sided power spectral density of the thermal noise.

3.3 Temporal Pulse Slot Representation

Our receiver performance analysis assumes that only the pulse slots immediately adjacent to the pulse slot under detection will contain significant ISI contributions. Figure 7 illustrates the temporal pulse slot representation used where Ts_o contains the energy of the pulse under r

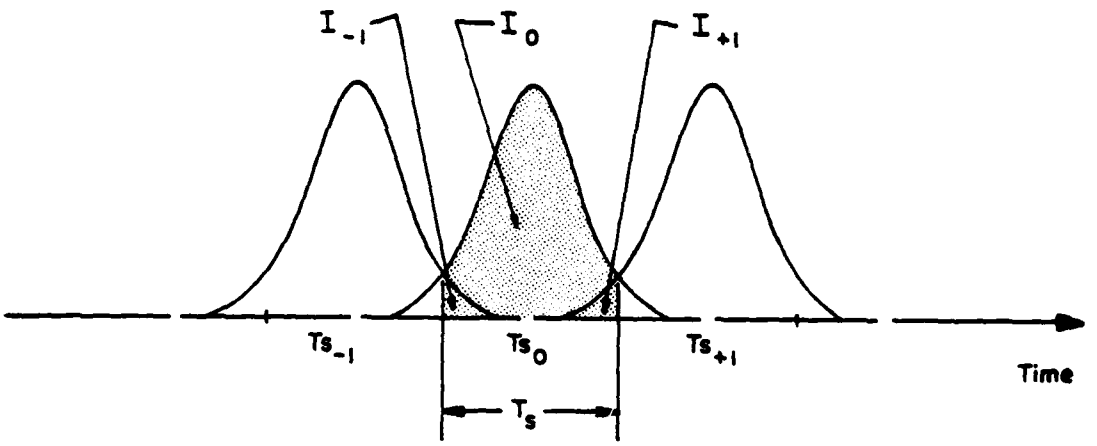

Figure 7. Temporal pulse slot representation.

detection. The energy in Ts_{+1} is integrated, sampled and dumped exactly one period before the energy in Ts_o is analyzed. Exactly one period after the energy in Ts_o is integrated, sampled and dumped, the energy in Ts_{-1} is analyzed. In Figure 7, I_o equals the energy in Ts due to the pulse under detection. I_{-1} and I_{+1} are the energies in Ts_o due to the temporal spreading of pulses in Ts_{-1} and Ts_{+1} respectively. The I_i energies are described in integral form by

$$I_o = \int_{t-\frac{T_s}{2}}^{t+\frac{T_s}{2}} d\tau \, d_o \, \langle |S_o(\tau)|^2 \rangle \Big|_{t=0} \tag{3.24}$$

$$I_{-1} = \int_{t-\frac{T_s}{2}}^{t+\frac{T_s}{2}} d\tau \, d_{-1} \, \langle |S_o(\tau + T_s)|^2 \rangle \Big|_{t=-T_s} \tag{3.25}$$

$$I_{+1} = \int_{t-\frac{T_s}{2}}^{t+\frac{T_s}{2}} d\tau \, d_{+1} \, \langle |S_o(\tau - T_s)|^2 \rangle \Big|_{t=T_s} \tag{3.26}$$

.

3.4 Expression for the Probability of Error

Amplitude shift keying is chosen to modulate the light intensity in the fiber. The linear receiver filter and sampling circuitry comprise an integrate-and-dump detection scheme [8]. The signal y(t), in Figure 6, is sampled every T_s seconds, where T_s is the temporal pulse slot width, which is inversely proportional to the bit rate. The sampled signal, $y(T_s)$, is the sum of a signal component s, and a noise component n. s is due to the signal induced shot noise in time slot Ts_o when a 1 is transmitted. n is comprised of thermal noise, and the shot noise components spilling over from adjacent time slots Ts_{-1} and Ts_{+1}. The dark current primary electron count is assumed to be small, and is

therefore neglected in this analysis. $y(T_s)$ is then compared to a decision threshold, r_T. If $y(T_s)$ is greater than r_T, the receiver decides a 1 was transmitted. If $y(T_s)$ is less than r_T, the receiver decides a 0 was transmitted.

We will temporarily neglect ISI effects and examine the two ways in which errors occur. If a 1 is transmitted, an error occurs if

$$s + n \leq r_T \tag{3.27}$$

where n is comprised of shot noise and thermal noise. An error will also occur if

$$n > r_T \tag{3.28}$$

when a 0 is transmitted. In this case, n is composed only of the thermal noise present in Ts_o. Since 0's and 1's are equally likely, the average probability of error can be given by

$$\begin{aligned} P(e) &= P(e|1)\cdot P(1) + P(e|o)\cdot P(o) \\ &= \tfrac{1}{2} P(s + n \leq r_T) + \tfrac{1}{2} P(n > r_T). \end{aligned} \tag{3.29}$$

Our error analysis concentrates on the energies in time slots Ts_o, Ts_{-1}, and Ts_{+1}, which give rise to eight possible probability of error combinations based upon 0's and 1's appearing independently in the three time slots under discussion. The total average probability of error can be expressed as

$$
\begin{aligned}
P(e) = {} & P(e|d_{-1}=1,\, d_{+1}=1)\cdot P(d_{-1}=1,\, d_{+1}=1) \\
& + P(e|d_{-1}=0,\, d_{+1}=1)\cdot P(d_{-1}=0,\, d_{+1}=1) \\
& + P(e|d_{-1}=1,\, d_{+1}=1)\cdot P(d_{-1}=1,\, d_{+1}=0) \\
& + P(e|d_{-1}=0,\, d_{+1}=0)\cdot P(d_{-1}=0,\, d_{+1}=0)\ .
\end{aligned}
\tag{3.30}
$$

Since d_i is a sequence of independent equiprobable data symbols and if we assume symmetric pulse shapes, then it can be shown that [9]

$$I_{+1} = I_{-1} = I_1 \tag{3.31}$$

and

$$
\begin{aligned}
P(e) = {} & \tfrac{1}{8}[P_A(e|d_o=0,d_{-1}=1,d_{+1}=1) + P_B(e|d_o=1,d_{-1}=1,d_{+1}=1] \\
& + \tfrac{1}{16}[P_C(e|d_o=0,d_{-1}=0,d_{+1}=1) + P_D(e|d_o=1,d_{-1}=0,d_{+1}=1)] \\
& + \tfrac{1}{8}[P_G(e|d_o=0,d_{-1}=0,d_{+1}=0) + P_H(e|d_o=1,d_{-1}=0,d_{+1}=0)]\ .
\end{aligned}
\tag{3.32}
$$

3.5 Gaussian Approximation for Shot Noise Distribution

If we approximate the shot noise distribution as Gaussian, the mean and variance of the process completely describe it. Further, the difficulty in evaluating an inhomogeneous nonstationary shot noise process is avoided. If we assume the avalanche gain of the APD is large, the Gaussian distribution is a good approximation to the exact distribution [10]. It can be shown [9] that the expression for the average probability of error, P(e), in (3.32) can be

expressed as

$$P(e) = \frac{1}{2} + \frac{1}{16}\left[\operatorname{erf}\left(\frac{\alpha_T - (1+2\Delta I)}{\sqrt{2\left(1 + \frac{2\Delta I}{N+1}\right)}}\ \mathrm{SNR}\right) - \operatorname{erf}\left(\frac{\alpha_T - 2\Delta I}{\sqrt{2\left(1 + \frac{2\Delta I - 1}{N+1}\right)}}\ \mathrm{SNR}\right)\right]$$

$$+ \frac{1}{8}\left[\operatorname{erf}\left(\frac{\alpha_T - (1+\Delta I)}{\sqrt{2\left(1 + \frac{\Delta I}{N+1}\right)}}\ \mathrm{SNR}\right) - \operatorname{erf}\left(\frac{\alpha_T - \Delta I}{\sqrt{2\left(1 + \frac{\Delta I - 1}{N+1}\right)}}\ \mathrm{SNR}\right)\right] \qquad (3.33)$$

$$+ \frac{1}{16}\left[\operatorname{erf}\left(\frac{\alpha_T - 1}{\sqrt{2}}\ \mathrm{SNR}\right) - \operatorname{erf}\left(\frac{\alpha_T}{\sqrt{\frac{2N}{N+1}}}\ \mathrm{SNR}\right)\right]$$

where dimensionless quantities have been introduced. A measure of the ISI is given by the spreading ratio

$$\Delta I = \frac{I_1}{I_o} \quad . \qquad (3.34)$$

We define the signal energy by

$$s = \frac{\eta}{hf}\,\bar{h}\,I_o \quad . \qquad (3.35)$$

The decision threshold, normalized by the signal energy, is given by

$$\alpha_T = \frac{r_T}{s} \quad . \qquad (3.36)$$

The ratio of thermal noise to shot noise is given by

$$N = \frac{\sigma_{th}^2}{\bar{h}s} = \frac{\text{thermal noise variance}}{\text{shot noise variance}} \quad . \qquad (3.37)$$

We define the signal-to-noise ratio (SNR) as

$$\text{SNR} = \frac{s}{(\sigma_{th}^2 + \bar{h}s)^{1/2}} = \frac{s^{1/2}}{\bar{h}^{1/2}(1 + N)^{1/2}} = \frac{\left[\frac{\eta}{hf} I_o\right]^{1/2}}{(1 + N)^{1/2}} \quad . \tag{3.38}$$

CHAPTER 4

RECEIVER OPTIMIZATION

4.1 Evaluation of the Optimum Decision Threshold

If the receiver is operating under the ideal conditions of zero thermal noise, zero ISI, and zero dark current, the resulting decision threshold would be equal to zero. A given time slot will contain energy only if a one is transmitted in that period. There will be no energy present in the time slot if a 0 is transmitted. Unfortunately, both thermal noise and ISI are present, forcing the decision threshold to be greater than zero. By optimizing this decision threshold, we can improve on error performance of the receiver.

A measure of the ISI is the spreading ratio, ΔI, discussed in the previous chapter. If we assume Gaussian pulse shapes, expressions can be easily derived for the pulse energies I_o and I_1 in terms of the error function and complementary error function [9]. The analytical expressions for the pulse energies are

$$I_o = \text{erf}\left(\frac{T_s}{2\sqrt{2}\ T_{out}}\right) \tag{4.1}$$

$$I_1 = \frac{1}{2}\ \text{erfc}\left(\frac{T_s}{2\sqrt{2}\ T_{out}}\right) . \tag{4.2}$$

We can express the spreading ratio in terms of T_s and T_{out} by

$$\Delta I = \frac{\frac{1}{2}\ \mathrm{erfc}\left(\frac{T_s}{2\sqrt{2}\ T_{out}}\right)}{\mathrm{erf}\left(\frac{T_s}{2\sqrt{2}\ T_{out}}\right)} \quad . \tag{4.3}$$

In Figure 8, the spreading ratio is plotted as a function of the ratio of signaling interval, T_s, to the rms output pulse width, T_{out}, for a Gaussian pulse shape.

To determine the optimum threshold, we will examine the two conditions under which a detection error is most likely to occur. The receiver is most likely to erroneously detect a 1 in Ts_o when both adjacent time slots contain 1's. Energy will spread into Ts_o from adjacent time slots due to ISI. Thermal noise will also increase the energy in Ts_o. If the ISI and thermal noise contributions are great enough, the decision threshold will be exceeded and the receiver will erroneously detect the presence of a 1 in Ts_o.

The receiver is most likely to decide a 0 was transmitted in Ts_o when a 1 was actually transmitted when the adjacent time slots both contain 0's. If the ISI is severe enough, excessive energy will spread into Ts_{-1} and Ts_{+1}, leaving an insufficient amount of energy in Ts_o to exceed the threshold.

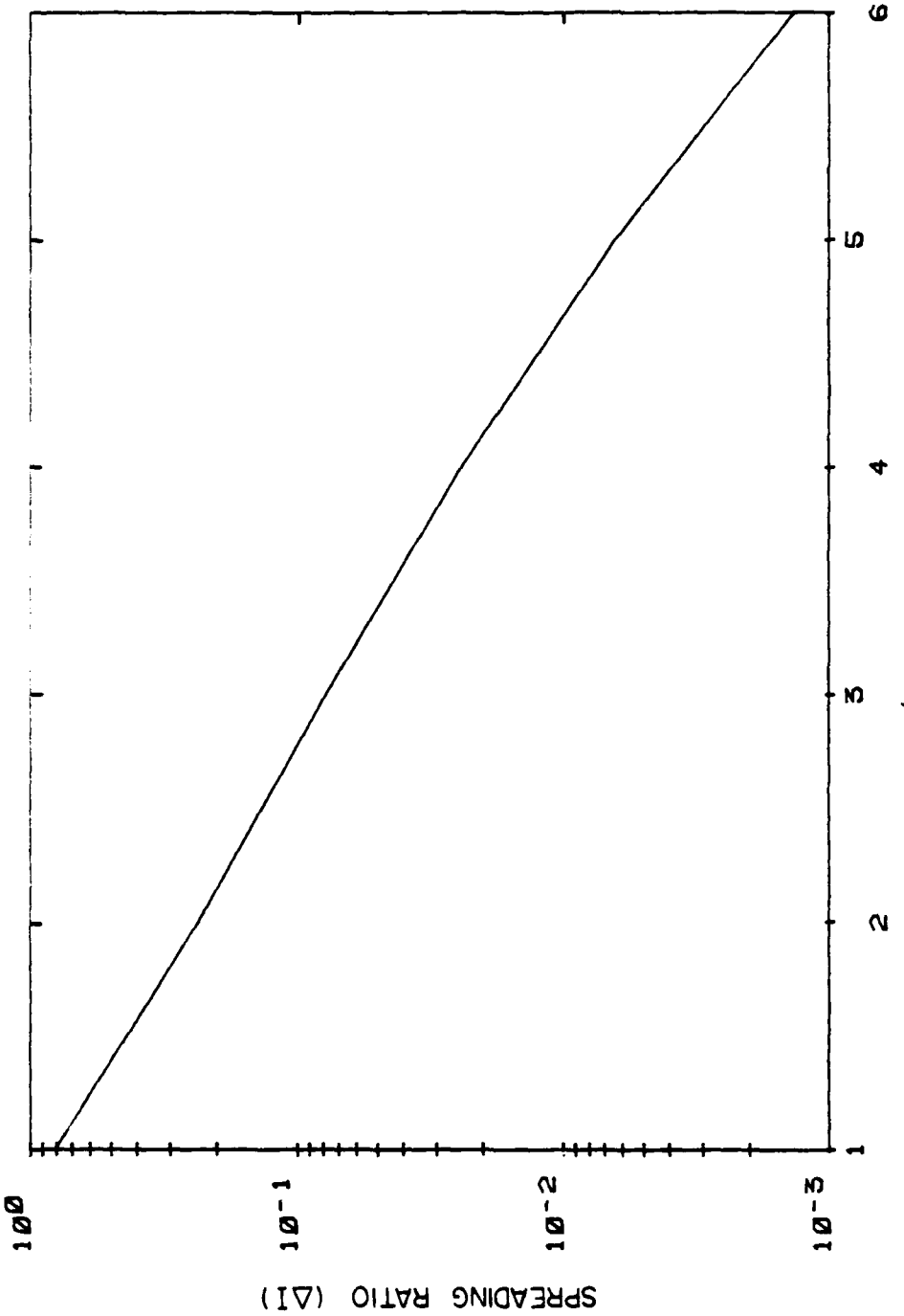

Figure 8. ISI spreading ratio as a function of the ratio of the signaling interval T_s to the rms output pulse width T_{out}.

An approximation for the probability of error can be found if these two worst case conditions are summed together in the expression

$$P(e) \simeq P_A(e|d_o = 0,\ d_{-1} = 1,\ d_{+1} = 1) + P_H(e|d_o = 1,\ d_{-1} = 0,\ d_{+1} = 0). \tag{4.4}$$

To determine the optimum threshold which minimizes P(e), we will differentiate (4.4) with respect to the normalized threshold, α_T, set the result equal to zero, and solve for the optimum threshold, α_{OPT}. The expression for the optimum threshold is

$$\alpha_{OPT} = \frac{N(2 - 4\Delta I) - (ab + c + d + e)^{1/2}}{4\Delta I - 2} \tag{4.5}$$

where

$$a = \Delta I(16\Delta I + 8N - 8) - 4N$$

$$b = \ln\left(1 + \frac{2\Delta I - 1}{N + 1}\right) / SNR^2$$

$$c = N^2(16\Delta I^2 - 16\Delta I + 4)$$

$$d = N(32\ \Delta I^3 - 16\Delta I^2 - 8\Delta I + 4)$$

$$e = 32\Delta I^3 - 32\Delta I^2 + 8\Delta I\ .$$

We see that in the absence of ISI and thermal noise, the optimum threshold reduces to zero as expected.

4.2 Numerical Results

In Figures 9-12, the optimum threshold, α_{OPT}, is plotted as a function of the spreading ratio, ΔI, for several values of the thermal noise to shot noise ratio, N. Values of N used are 0.0001, 1.0, 2.0, and 3.0 in each figure. The SNR is held constant for each set of curves. The advantage of increasing the signal strength is evident if we compare Figure 12 with Figure 9 and note the significantly lower values of optimum threshold when a strong signal is present.

In Figures 13-16, the optimum threshold is plotted as a function of the spreading ratio for several values of SNR. The value of the thermal noise to shot noise ratio, N, is held constant for each set of curves. For values of N greater than 0.5, the value of the optimum threshold increases linearly with increasing values of ΔI. For small values of N the relationship between α_{OPT} and ΔI is very nonlinear. Under these conditions, very small optimum threshold values can be realized for low ISI levels.

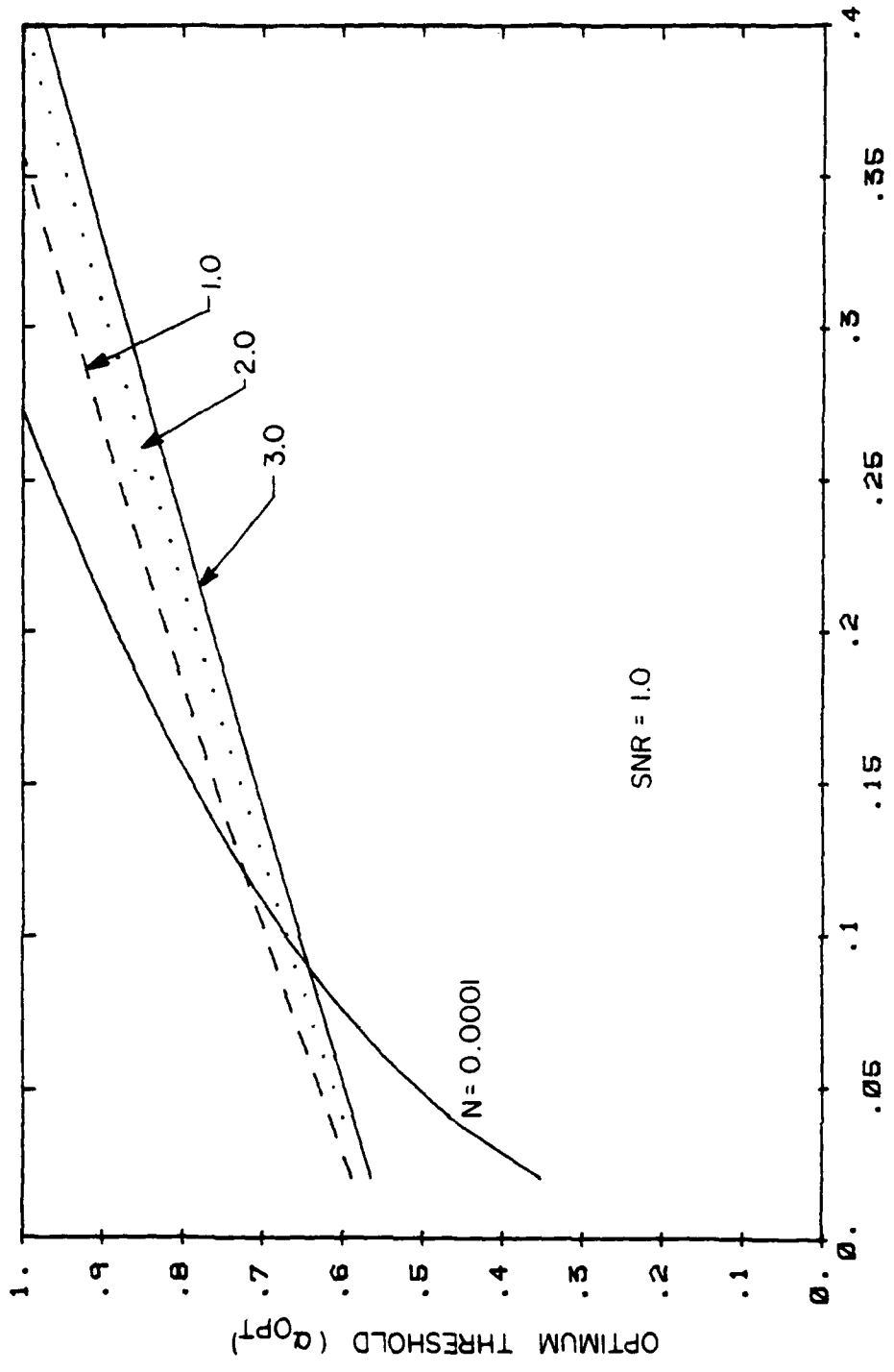

Figure 9. Optimum threshold as a function of the ISI spreading ratio for a Gaussian shot noise distribution. SNR is held constant.

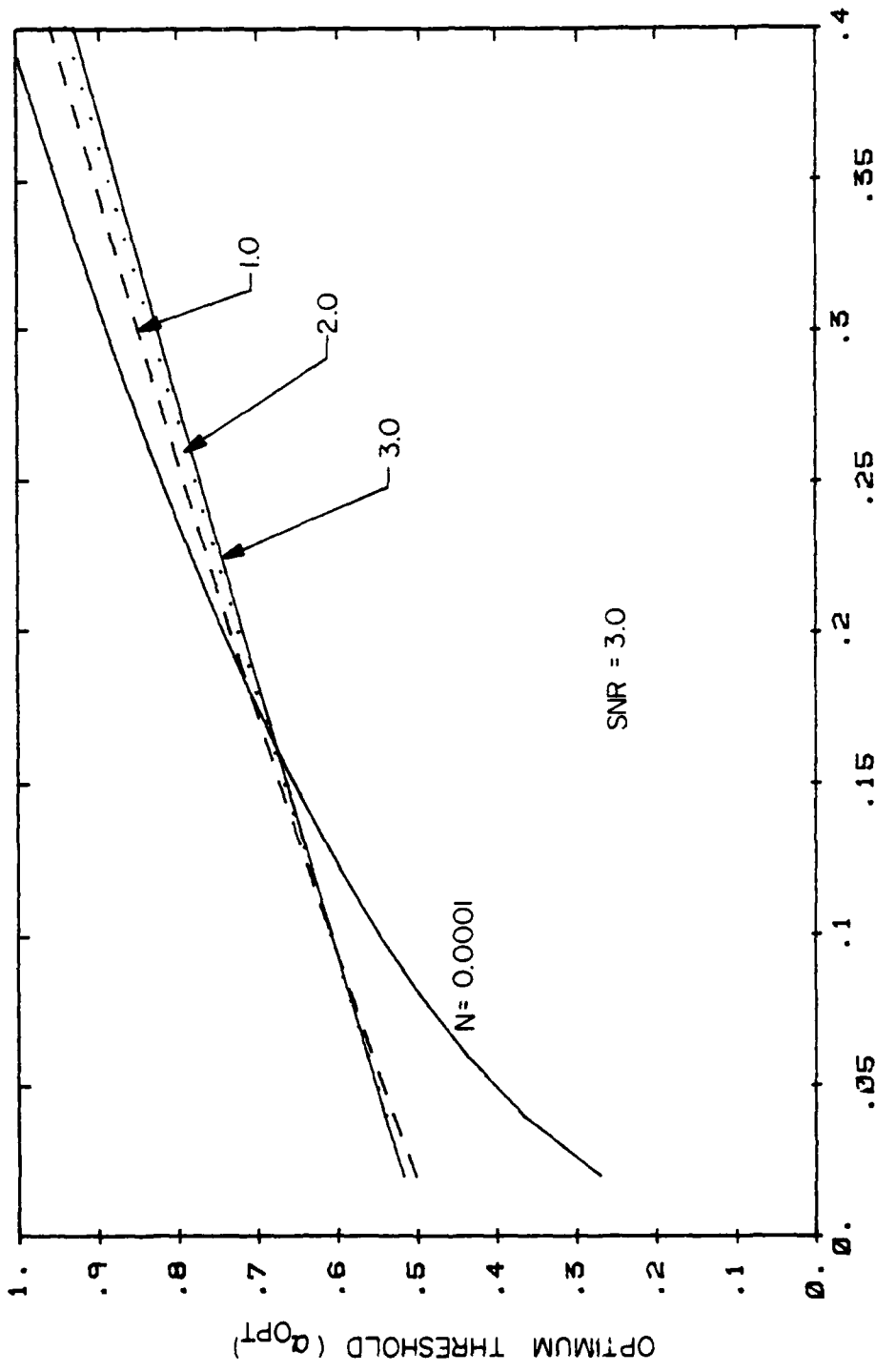

Figure 10. Optimum threshold as a function of the ISI spreading ratio for a Gaussian shot noise distribution. SNR is held constant.

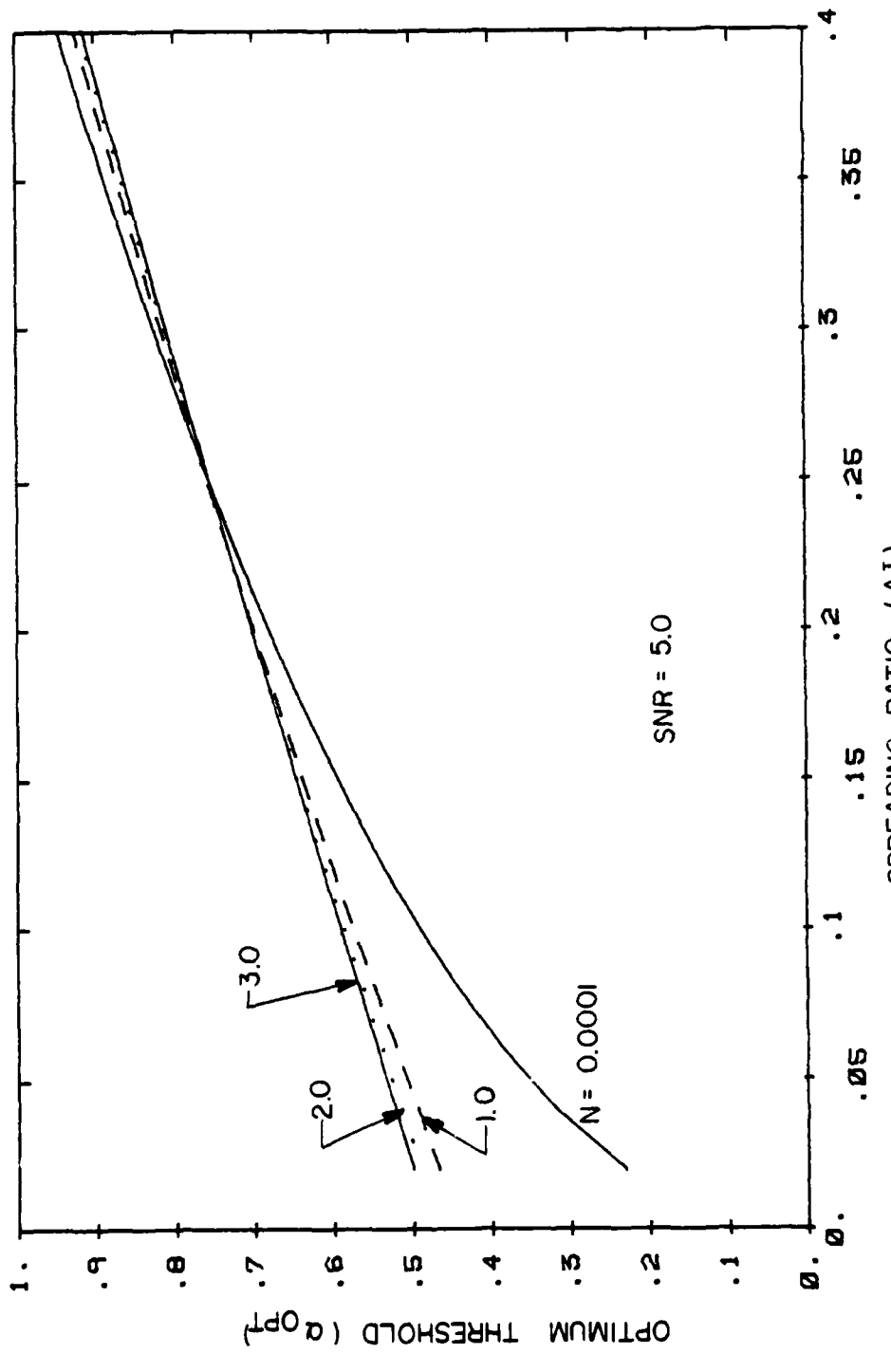

Figure 11. Optimum threshold as a function of the ISI spreading ratio for a Gaussian shot noise distribution. SNR is held constant.

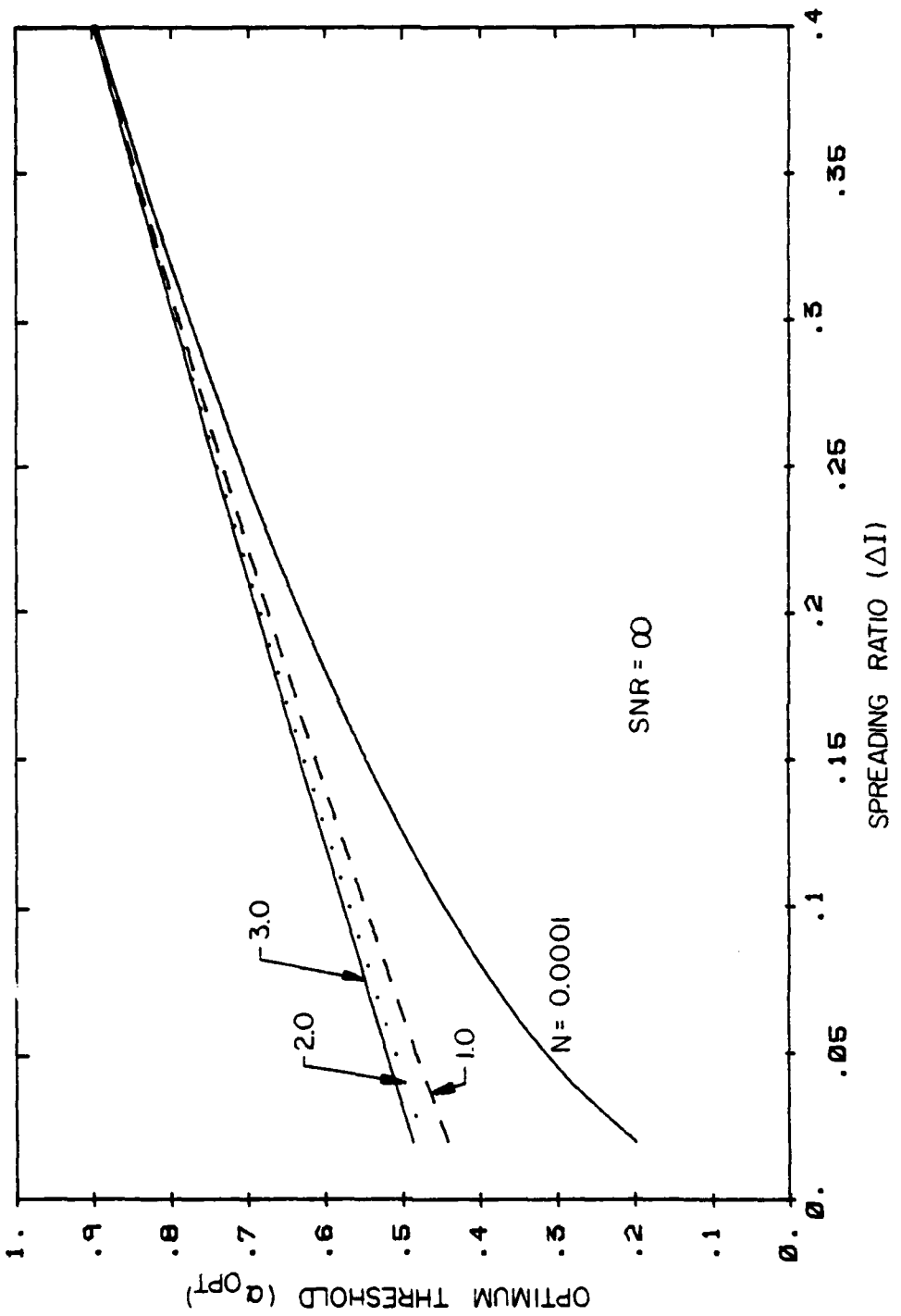

Figure 12. Optimum threshold as a function of the ISI spreading ratio for a Gaussian shot noise distribution. SNR is held constant.

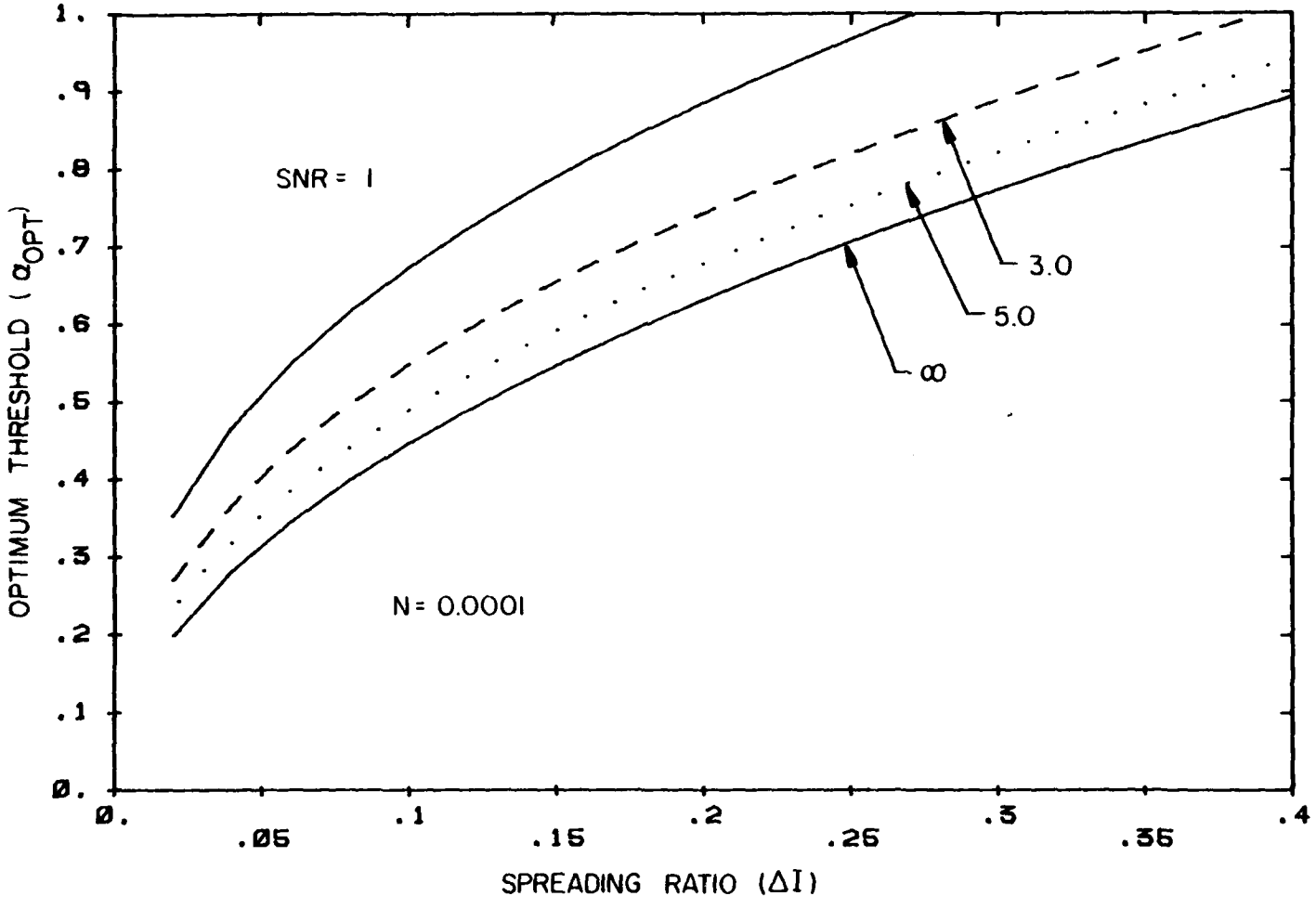

Figure 13. Optimum threshold as a function of the ISI spreading ratio for a Gaussian shot noise distribution. N is held constant.

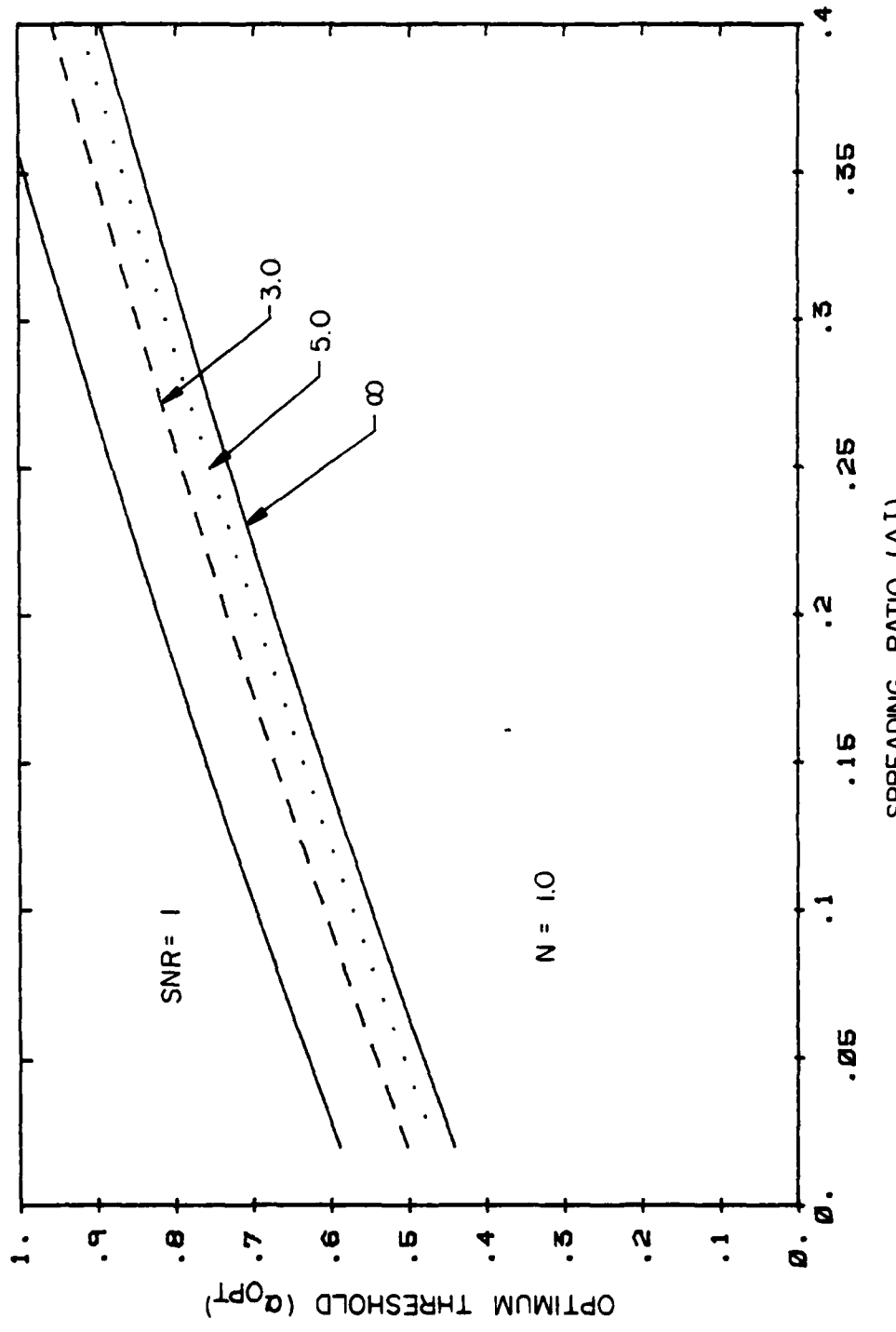

Figure 14. Optimum threshold as a function of the ISI spreading ratio for a Gaussian shot noise distribution. N is held constant.

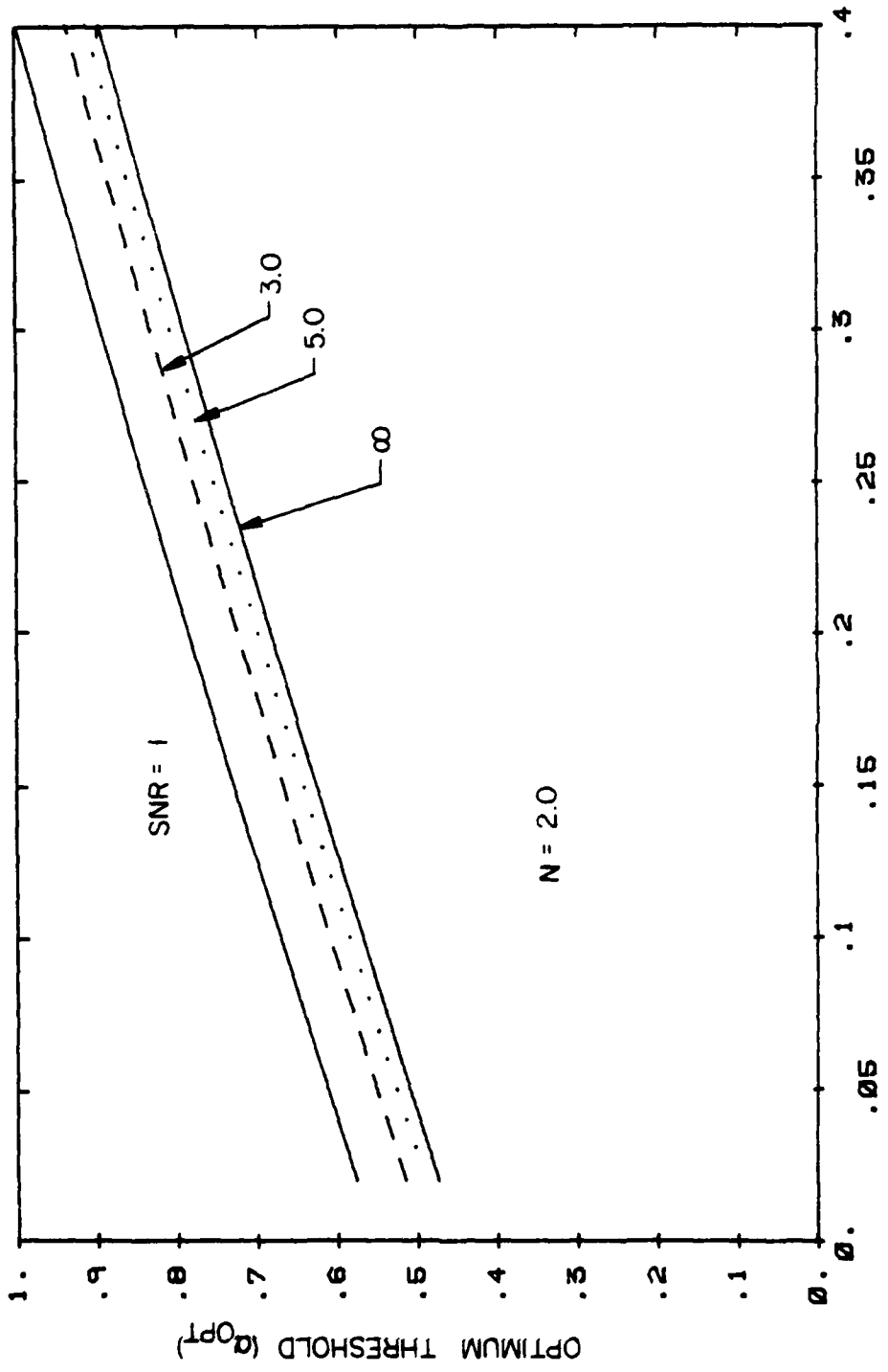

Figure 15. Optimum threshold as a function of the ISI spreading ratio for a Gaussian shot noise distribution. N is held constant.

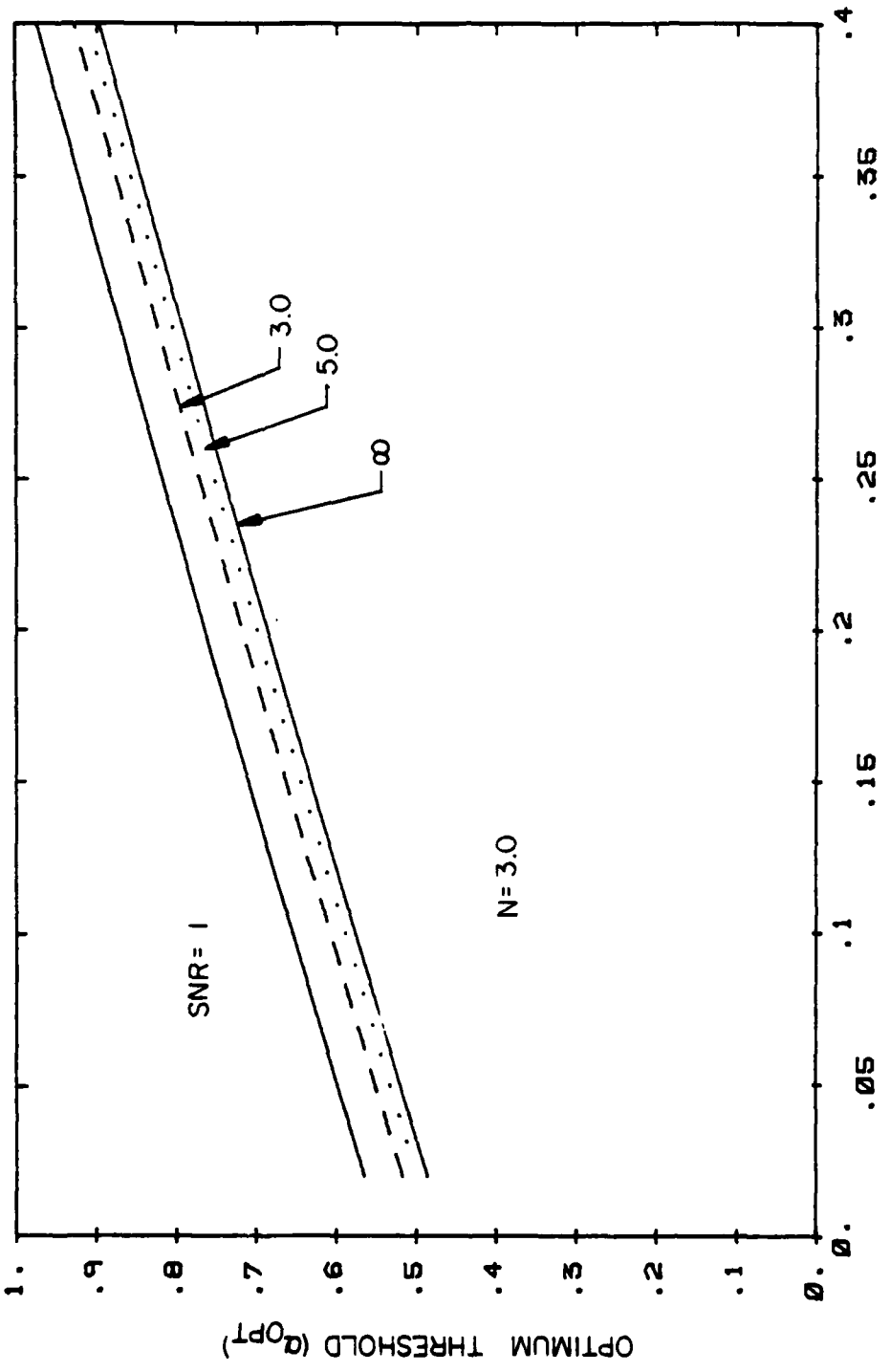

Figure 16. Optimum threshold as a function of the ISI spreading ratio for a Gaussian shot noise distribution. N is held constant.

CHAPTER 5

RECEIVER PERFORMANCE AND SYSTEM DESIGN CONSIDERATIONS

5.1 Receiver Error Rate Performance

Since we have expressions for the probability of error (3.33), and the optimum decision threshold, (4.5), we can replace α_T in (3.33) by α_{OPT} to obtain an expression for P(e) which is minimized for the variables, ΔI, SNR, and N. If the communications system is designed such that the spreading ratio, ΔI, is zero, P(e) becomes a function of N and SNR only and is shown in Figure 17. The error probability is a monotonically decreasing function of the signal-to-noise ratio. For a constant signal-to-noise ratio, the error probability increases with increasing values of N which corresponds to an increase in the thermal noise. Also, to maintain a specified error rate of 10^{-8}, the SNR must increase by approximately 2.5 dB if the noise ratio increases from 10^{-4} to 10.0.

In Figures 18-21, P(e) is plotted versus ΔI, SNR, and N when the intersymbol interference is not zero. Again, the error probability decreases monotonically as a function of the signal-to-noise ratio. N is held constant for each plot and takes on values of 10^{-4}, 0.1, 0.5, and 10.0 for successive figures. In each plot, P(e) is shown for I = 0.01, 0.1, 0.2, and 0.3. A review of Figures 18-21 indicates that

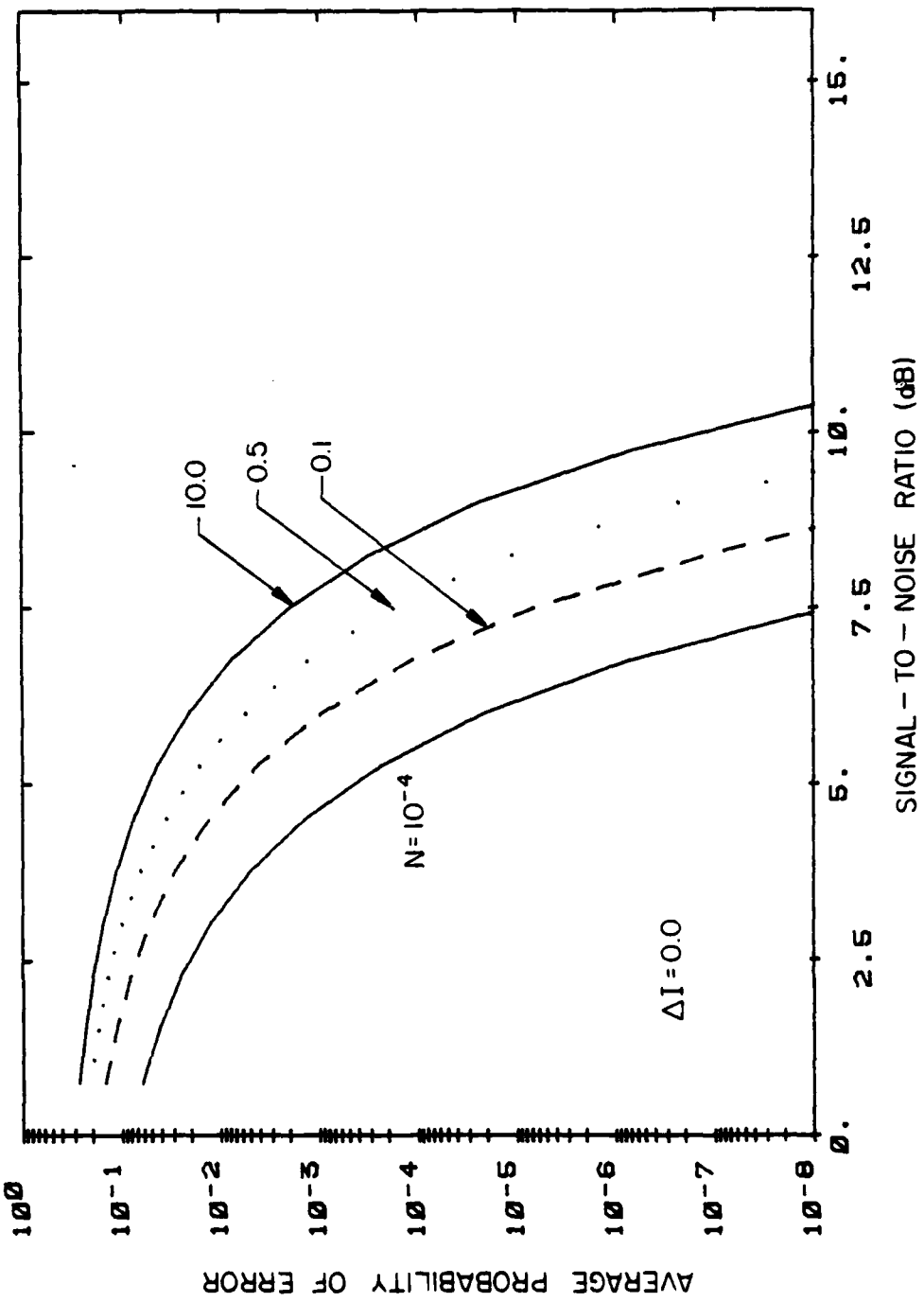

Figure 17. Average probability of error as a function of the signal-to-noise ratio for various values of N and zero ISI.

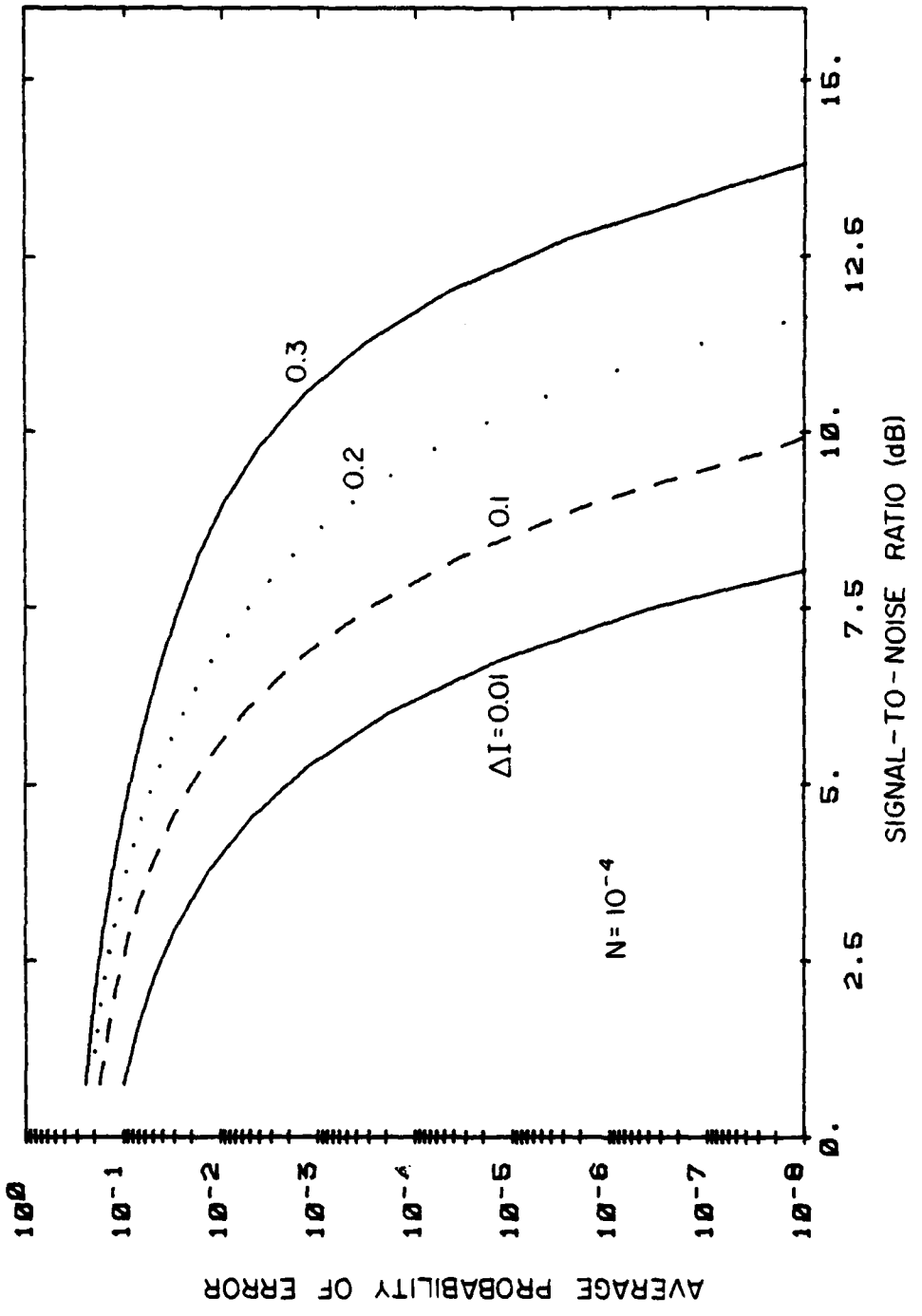

Figure 18. Average probability of error as a function of the signal-to-noise ratio for various values of the spreading ratio with N held constant.

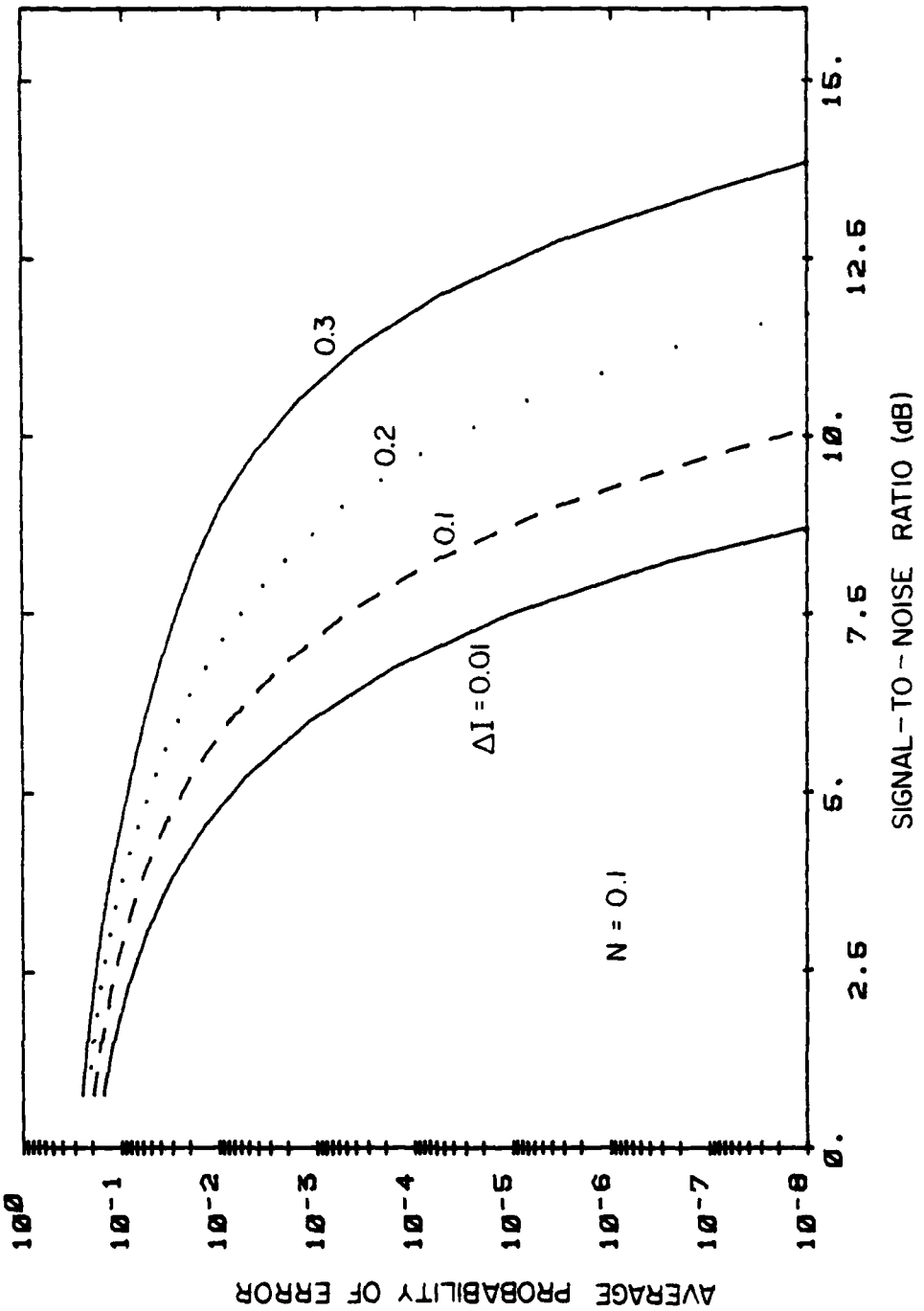

Figure 19. Average probability of error as a function of the signal-to-noise ratio for various values of the spreading ratio with N held constant.

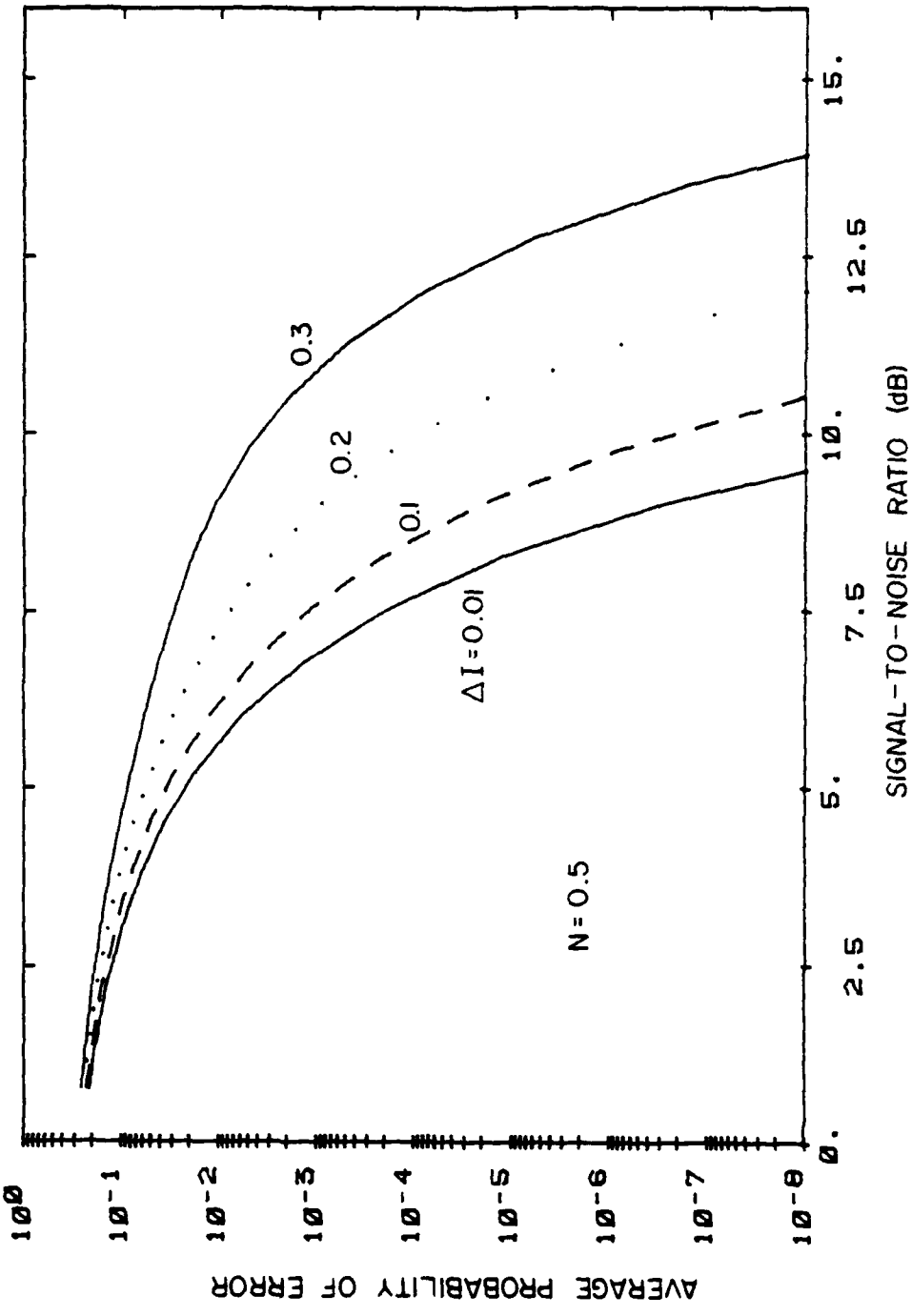

Figure 20. Average probability of error as a function of the signal-to-noise ratio for various values of the spreading ratio with N held constant.

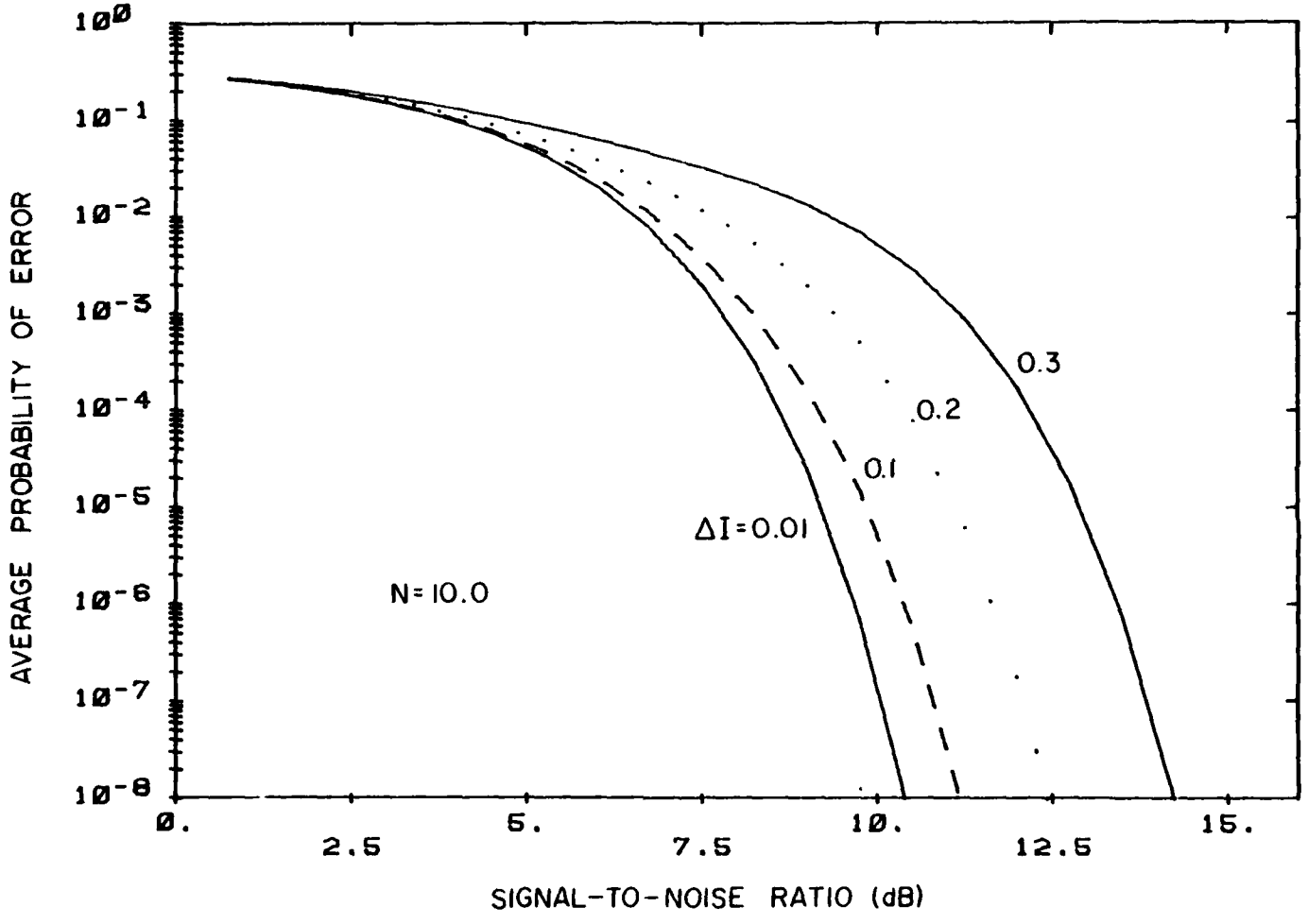

Figure 21. Average probability of error as a function of the signal-to-noise ratio for various values of the spreading ratio with N held constant.

the spreading ratio has a much greater effect upon the error probability at low noise levels. Thus, when designing an optical fiber communications system with a specified error rate, controlling the ISI becomes more important at low noise levels.

5.2 System Design Considerations

When designing an optical fiber communications system, the error probability is of primary importance and is normally one of the initial specifications. A typical value of N can be obtained for available receivers. Knowing the error probability and N, and by referring to Figures 18-21, a maximum value for ΔI can be obtained once we specify an appropriate SNR based upon the system parameters. In Figure 8, we can obtain a value for T_s/T_{out} for this value of ΔI. Specifying the bit rate now allows us to calculate the value for T_{out}. Knowing the maximum allowable value of T_{out}, and the desired optical fiber cable length further specifies the value for the rms input pulse width. We can now select the proper fiber and source in order to meet the requirements for the optical fiber system.

CHAPTER 6

CONCLUSION

In this report we have analyzed the effects of pulse dispersion and intersymbol interference on the performance of a graded-index fiber optic communication system. By using the WKB approximation, it was found that with the proper choice of the index gradient, α, modal dispersion can be reduced such that material dispersion is the dominant factor in calculating pulse dispersion in a graded-index fiber.

An expression for the rms output pulse width, T_{out}, was developed in terms of the dispersion parameters, the length of the fiber, and the rms input pulse width, T_i. It was shown that a narrow linewidth source, such as a laser, is capable of achieving a smaller T_{out} than an LED with an equivalent value for T_i. We also find that for small values of T_i, the pulse underwent severe temporal spreading, which resulted in T_{out} being many times greater than T_i.

A mathematical model of an optical digital receiver was developed using an APD as the optical detector and an integrate-and-dump pulse detection scheme. Dark current was considered negligible and a Gaussian approximation was made for the shot noise. An expression for the optimum decision threshold of the receiver was developed in terms of the SNR,

the thermal noise to shot noise ratio, and the spreading ratio, ΔI. We have shown that a linear relationship exists between α_{OPT} and ΔI when N is greater than 1.0. In general we have shown that α_{OPT} increases with increasing values of N and ΔI. Also, α_{OPT} decreases with increasing values of SNR.

An expression for the average probability of error was developed for the system as a function of the optimum decision threshold, the spreading ratio, the thermal noise to shot noise ratio, and the SNR. In general the error rate increases for increasing values of N and ISI, while decreasing for increasing values of the SNR. Also, ISI has a more pronounced effect on the error rate at low noise levels when compared to the situation at high noise levels.

In the final section, we developed a method of designing a fiber optic communication system based upon the preceding analysis. Using this method, an appropriate selection of the optical source and fiber optic cable can be made based upon the system specifications.

REFERENCES

[1] Jefferies, J. A., and Klaiber, R. J., "Lightguide theory and its implications in manufacturing," The Western Electric Engineer, vol. 24, no. 1, pp. 13-24, Winter 1980.

[2] Olshansky, R., and Keck, D., "Pulse broadening in graded-index optical fibers," Applied Optics, vol. 15, no. 2, pp. 483-491, February 1976.

[3] Midwinter, J. E., "Optical Fibers for Transmission," New York: Wiley Company, 1979.

[4] Oyamada, K., and Okoshi, T., "High-accuracy WKB analysis of α-power graded-core fibers," IEEE Trans. Microwave Theory & Tech., pp. 839-845, August 1980.

[5] Rugemalira, R. A. M., "The calculation of average error probability in a digital fiber optical communications system," Optical and Quantum Electronics, vol. 12, pp. 131-141, 1980.

[6] Personick, S. D., "Receiver design for digital fiber optic communications systems, I," Bell System Technical Journal, vol. 52, no. 6, pp. 843-874, July-August 1973.

[7] Papoulis, A., "Estimation of the average density of a nonuniform Poisson process," IEEE Trans. Comm., vol. COM-22, no. 2, pp. 162-167, February 1974.

[8] Ziemer, R. E., and Tranter, W. H., Principles of Communications: Systems, Modulation and Noise. Boston: Houghton Mifflin Company, 1976.

[9] Picini, F. M., "Intersymbol interference in digital fiber optic communication systems," Master's Thesis, University of Illinois, 1981.

[10] Barnosky, M. K., Fundamentals of Optical Fiber Communications, New York: Academic Press, Inc., 1976.


DAT
ILM